VNIVERSITAT DE VALÈNCIA

Optical Impact of Correcting Elements

PROGRAMA DE DOCTORADO
EN OPTOMETRÍA Y CIENCIAS DE LA VISIÓN

Doctorando:
Georgios Zoulinakis

Directora de Tesis:
Teresa Ferrer Blasco

Burjassot, Noviembre de 2016

VNIVERSITAT DE VALÈNCIA

Optical Impact of Correcting Elements

PROGRAMA DE DOCTORADO EN OPTOMETRÍA Y CIENCIAS DE LA VISIÓN

Doctorando:

Georgios Zoulinakis

Directora de Tesis:

Teresa Ferrer Blasco

Burjassot, Noviembre de 2016

Optical Impact of Correcting Elements

Memoria presentada por

Georgios Zoulinakis

Para optar al grado de

DOCTOR en OPTOMETRÍA Y CIENCIAS DE LA VISIÓN

This project has received funding from the European Union's FP7 research and innovation program under the Marie Curie Initial Training Network AGEYE (FP7-PEOPLE-ITN-2013), grant agreement No 608049.

DECLARATION

No portion of the work referred to in the thesis has been submitted in support of an application for another degree or qualification of this or any other University or other institution of Learning.

Dña. Teresa Ferrer Blasco de la Universidad de Valencia CERTIFICA que la presente memoria “Optical impact of correcting elements”, resume el trabajo de investigación realizado, bajo su dirección, por D. Georgios Zoulinakis y constituye su Tesis para optar al Grado de Doctor en Optometría y Ciencias de la Visión.

Y para que así conste, y en cumplimiento de la legislación vigente, firma el presente certificado en Valencia, a Noviembre de dos mil dieciséis.

Fdo. Teresa Ferrer Blasco

Acknowledgements:

Θα ήθελα να ευχαριστήσω πρώτα απ' όλους την οικογένεια μου για την υποστήριξη και την υπομονή τους στον δρόμο που διάλεξα να ακολουθήσω.
(First of all I would like to thank my family for their support and patience in the path that I chose to follow.)

In this part I would like to thank all my colleagues, teachers and supervisors in University of Valencia and in the AGEYE project that provided any kind of help or knowledge that helped me in the completion of the present thesis.
I would like to thank my supervisors from University of Valencia, Dr. Teresa Ferrer Blasco and Prof. Robert Montés Micó, for their help and support in this project.
I would also like to thank Prof. D. Robert Iskander from Wroclaw University of Science and Technology (Polytechnica Wrocławska) in Poland, who accepted me in his team for my secondment and supported me with his guidance and knowledge provided.
Closing, I would like to thank my colleague Antonio Jesús del Águila Carrasco, for his help in building the Matlab code that calculated the VSOTF in chapters 4, 5 and 6 of the present Thesis.

Resumen

La presente Tesis Doctoral, titulada “Optical impact of correcting elements”, forma parte de la Marie Curie Initial Training Network denominada AGEYE financiada por la Comisión Europea (FP7-PEOPLE-ITN-2013-608049).

El principal objetivo de esta Tesis es el estudio y la investigación de elementos correctores que son utilizados con el fin de compensar errores refractivos y patología que aparecen con el envejecimiento. Se busca el desarrollo de modelos mediante simulaciones con el fin de conocer el impacto de dichos elementos ópticos que son aplicados en las alteraciones oculares propias de la edad con el fin de proponer alternativas a las soluciones que existen actualmente. Dichas alteraciones son la presbicia y las cataratas, ambas presentes entre los 40 y los 60 años de edad. La presbicia es la imposibilidad de acomodar a objetos en distancias próximas, por ejemplo, a la distancia de lectura, y las cataratas la opacificación del cristalino. Igualmente la degeneración macular asociada a la edad es una de las alteraciones a considerar con el envejecimiento.

Los elementos correctores que se utilizan en tales patologías son las lentes de contacto (LC) y las lentes intraoculares (LIO). Estos son los elementos que se diseñan y estudian en esta Tesis. Estos elementos pueden ser monofocales, multifocales con diferentes zonas de refracción o patrones de difracción, fabricados con diferentes materiales y revestidos con diferentes filtros para absorber algunas partes del espectro de luz (como el espectro ultravioleta). Todos los estudios que se presentan en esta Tesis son estudios de simulación. Esto significa que todos los "experimentos" fueron diseños ópticos en el entorno de programación mediante dos programas.

El primer programa es un programa de diseño óptico que se utiliza comúnmente por ingenieros ópticos para diseñar sistemas ópticos tales como cámaras, telescopios y cualquier elemento que incluya partes ópticas. Como tal, puede ser utilizado para diseñar el sistema óptico del ojo humano, componiéndolo a partir de diferentes lentes que están en contacto entre ellas. Estas lentes pueden ser la córnea, la cámara anterior con el humor acuoso, el cristalino y el humor vítreo. Todos estos elementos pueden ser diseñados y puestos conjuntamente para crear un modelo de ojo humano. Elementos de corrección

como LCs y LIOs también pueden ser diseñados y agregados en este sistema óptico. Se pueden incluir datos de personalización, como topografías y mediciones biométricas, para crear un modelo de ojo personalizado y realizar estudios basados en datos específicos o en grupos de diferentes modelos de ojos para su análisis estadístico.

El segundo programa, es un programa comúnmente utilizado para el análisis matemático, estadísticas y lo que incluye el análisis matemático basado en matrices. Se utilizó para diseñar un código personalizado (desarrollado por Georgios Zoulinakis) que podría diseñar patrones difrativos de LIOs y producir archivos de texto con datos. Estos datos se pueden implementar en el software de trazado de rayos y éste es capaz de utilizar los datos y el diseño de la LIO difractiva que luego se implanta en un modelo de ojo. Este código personalizado se usó en el capítulo 3 de la Tesis para crear lentes esféricas y asféricas y comprobar así los resultados con las lentes que el software de diseño óptico estaba diseñando por sí misma. Después de eso, fue utilizado en el capítulo 5 para diseñar LIOs difractivas que se utilizaron en ese estudio. Una descripción del código se da en el apéndice A. Se utilizó un segundo código personalizado (desarrollado por los profesores D. Robert Iskander y Larry Thibos) en los capítulos 4 y 5. Este código puede calcular la relación visual de Strehl basada en la función de transferencia óptica (VSOTF) de un modelo de ojo humano. Matlab también se utilizó para el análisis estadístico en los capítulos 4 y 5, aunque los gráficos se hicieron en Microsoft Excel (Microsoft).

En la presente Tesis no se tomaron medidas de pacientes o animales. En los capítulos 4 y 5, se utilizaron datos retrospectivos de pacientes recogidos con anterioridad, siguiendo en este caso los principios de la Declaración de Helsinki y tiendo consentimiento por escrito de todos los participantes. En todo el contenido de la presente Tesis se diseñan y examinan elementos de corrección tales como LCs y LIOs. Estos elementos no están protegidos por derechos de autor, no son partes de patentes o elementos totalmente patentados. Están diseñados siguiendo características generales y utilizados sólo para simulaciones y extracción de resultados y conclusiones del uso de dichos elementos. La presente Tesis está compuesta por 7 capítulos y dos apéndices. A continuación se dará una descripción detallada de cada uno de los capítulos.

El primer capítulo incluye la introducción en el campo de investigación de la Tesis. Así, hay información del ojo humano y las partes de las que está compuesto. Hay información biológica sobre sus partes y funciones y se explica la función de acomodación. Se describen

la presbicia y las cataratas y se explica el efecto en la visión de ambas con el fin de entender por qué se necesita esta investigación específica. Se presenta una lista de elementos correctores oculares y métodos para compensar estos defectos. Hay más información para LCs y LIOs ya que estos elementos son la herramienta principal de la presente Tesis. Al final de este capítulo hay una descripción del procedimiento de modelado del ojo humano. Se explica cómo se diseñan los modelos de los ojos en los programas de diseño óptico y cómo se utilizan. También se explica cómo los elementos correctores ópticos, tales como LCs y LIOs, pueden ser diseñados y añadidos en estos modelos de ojo para ser estudiados.

El segundo capítulo contiene el primer estudio de esta Tesis. Se trata de un estudio sobre los diferentes modelos teóricos de ojos y una comparación entre ellos. En este estudio, se diseñaron tres modelos teóricos del ojo humano. Estos modelos fueron el modelo de ojo de Navarro, el modelo de ojo de Arizona, que es acomodativo usando funciones matemáticas para alterar sus características geométricas y el modelo de Liou-Brennan, que es un modelo de ojo más anatómico basado en valores promedios de sus parámetros. El modelo de Liou-Brennan tiene una característica más, que es el índice de refracción del gradiente del cristalino. Los otros dos modelos utilizan un solo índice de refracción del valor medio para el cristalino. Estos tres modelos de ojo humano fueron diseñados utilizando el programa de diseño óptico y siguiendo los métodos de diseño de sus creadores en los artículos publicados.

El objetivo principal de este estudio fue comparar los resultados producidos por estos modelos en procedimientos estáticos y acomodativos. Para los procedimientos acomodativos, la distancia del test se cambió para cuatro posiciones diferentes (infinito, 3 m, 1 m y 0,5 m). También se modificaron los parámetros geométricos de los modelos oculares. Estos incluyen radios de curvatura anterior y posterior para las superficies del cristalino, grosor del cristalino y profundidad de la cámara anterior. También hubo una disminución del diámetro de la pupila cuando el test se acercó con el fin de simular completamente el proceso de acomodación. Para el modelo de Arizona utilizamos las funciones matemáticas que están cambiando sus características geométricas. Para los otros dos modelos se utilizaron valores promedios que se encontraron en la bibliografía. Al final, los tres modelos de ojos se optimizaron para centrarse perfectamente en el test. La optimización se realizó con la herramienta de optimización y la variable de optimización se estableció como la profundidad o espesor del vítreo. Si un modelo de ojo no pudiera

acomodar correctamente, un gran cambio en el espesor del vítreo sería el resultado de la optimización. Al final, los tres modelos podían simular el procedimiento de acomodación con éxito. Si se tiene que proponer un modelo de ojo a partir de este estudio, éste podría ser el Liou-Brennan debido al índice de refracción del gradiente del cristalino. La elección final está en manos del investigador y su objetivo principal y no hay una mejor opción para proponer.

El tercer capítulo contiene el segundo estudio de esta Tesis. En este estudio hay una investigación sobre el diseño de una LIO monofocal. Más específicamente, la investigación tiene dos proyectos diferentes. En el primer proyecto se prueba la distribución de potencia dióptrica entre las superficies anterior y posterior de la LIO. Esto se hizo porque nos gustaría tener una referencia principal para los diseños de nuestros próximos estudios. Para este proyecto se eligió el modelo de Navarro por su simplicidad. El cristalino del modelo del ojo se eliminó y en su lugar se creó un espacio vacío. A este espacio se le dio el índice de refracción del humor acuoso, espacio que llena en realidad cuando se retira el cristalino. En este espacio se introdujeron las LIOs para este proyecto. Todas las LIOs fueron diseñadas con el código personalizado Matlab que se describe en el apéndice A y los resultados se compararon con las lentes diseñadas con el fin de probar los resultados producidos por el código.

Las LIOs fueron diseñadas con una potencia dióptrica total de -10, 10, 20, 30 y 40 D. La distribución de potencia en la superficie anterior de cada LIO fue del 0%, 25%, 50%, 75% y 100% de la potencia total. La superficie posterior tenía el resto de la potencia total de la LIO. Después de diseñar las LIOs, se optimizaron los modelos oculares con la herramienta de optimización y como variable de optimización se eligió el espesor del vítreo. Esto se realizó con el fin de probar el impacto óptico de la distribución de potencia de la LIOs en modelos de ojo perfectamente optimizados, de modo que cualquier diferencia en los resultados fue debida a la diferencia de distribución de potencia. El resultado fue que una potencia del 75% de la potencia dióptrica total se debe dar en la superficie anterior, especialmente para LIOs de potencias altas (30 y 40 D) con el fin de obtener mejores resultados ópticos.

En la segunda parte de este estudio se diseñaron LIOs con el 70%, 75% y 80% del poder dióptrico total en la superficie anterior. El modelo del ojo de Navarro se utilizó otra vez. El objetivo principal de este proyecto fue probar en cuál de las superficies de la LIO (anterior o posterior) las asfericidades de la LIO tenían que diseñarse para obtener mejores

resultados ópticos. La constante cónica y la asfericidad de segundo orden se diseñaron y optimizaron en la superficie anterior y posterior de cada LIO (de cada potencia dióptrica total) y para cada distribución de potencia. La calidad óptica fue comprobada y comparada. El resultado de esta parte fue que las asfericidades deben diseñarse en la superficie anterior de la LIO. Si la superficie posterior tiene que ser elegida entonces más órdenes de asfericidad deben ser implementados en el diseño óptico. En conclusión, este estudio mostró que entre el 70% y el 80% de la potencia dióptrica total tiene que ser dada en la superficie anterior de la LIO y las asfericidades tienen que ser diseñadas en la superficie anterior de la LIO también.

El cuarto capítulo contiene el tercer estudio de la presente Tesis. Este es un estudio sobre combinaciones de LIOs monofocales y LCs en modelos de ojos personalizados. El objetivo principal de este estudio fue comprobar si la optimización de las LIOs monofocales (LIOs optimizadas) o LCs tiene que considerarse o un diseño más robusto (no personalizado) también es eficiente para corregir adecuadamente los errores de refracción. El segundo objetivo fue comparar los resultados ópticos y visuales de combinaciones de elementos correctores (LC y LIO) con los resultados de una sola LIO, ya sea optimizada o no optimizada. El tercer y último objetivo fue comprobar la tolerancia de todos estos sistemas ópticos en situaciones de desalineación de la LIO. Tales desalineamientos eran descentramientos e inclinaciones de la LIO. El modelo de ojo teórico de Liou-Brennan se utilizó en este estudio. Para la personalización del modelo del ojo se modificó la superficie corneal anterior del mismo. Para ello, se utilizaron topografías corneales retrospectivas de 22 sujetos. Los datos topográficos corneales se introdujeron y procesaron con Matlab para obtener datos de coeficientes de Zernike para la córnea. Estos datos fueron introducidos en el software de trazado de rayos y al final se crearon 22 modelos de ojos personalizados

Los modelos oculares se dividieron en dos grupos, uno con córneas normales y el segundo con córneas astigmáticas (astigmatismo mayor de 0,75 D). De estos modelos de ojo se eliminó el cristalino y se diseñó un espacio vacío en su lugar. A este espacio vacío se le dio el índice de refracción del humor acuoso que llena este espacio cuando se éste se retira. Este espacio se utilizó para diseñar las LIOs asféricas monofocales. Se utilizó un método de diseño específico que añade componentes no secuenciales en el diseño secuencial del sistema óptico para facilitar la desalineación de la LIO posteriormente. Las LIOs optimizadas fueron diseñadas en primer lugar. Se utilizó la herramienta de optimización y las variables

de optimización fueron el segundo y cuarto orden de asfericidad y la constante cónica de la superficie anterior. Como resultado del estudio anterior (capítulo 3), la superficie anterior de cada LIO tenía un 75% de la potencia dióptrica total y las asfericidades se diseñaron en la superficie anterior de la LIO también. Los diseños robustos de LIOs dieron la potencia de la superficie anterior en pasos de 0,25 D. A los diseños robustos se incluyó un error de 0,25 D como error en el cálculo de la potencia de la LIO. Esto se implementó con el fin de simular un posible error de refracción inducido en el procedimiento quirúrgico. La potencia de la superficie posterior se fijó en 5D para todos los diseños. Las LCs optimizadas y robustas también fueron diseñadas en el software de trazado de rayos. También había una película lagrimal diseñada en el sistema óptico total entre la LC y la córnea. La LC no estaba tocando la córnea anterior de ningún modelo en ningún punto. Para proceder con los desalineamientos, todas las LIOs de todos los modelos fueron descentradas e inclinadas. El descentramiento fue en pasos de 0,25 mm y en magnitud total de 1 mm. Las inclinaciones fueron en pasos de 1 grado y en magnitud total de 5 grados. Todos los desalineamientos mencionados se realizaron en 8 direcciones diferentes, ya que los modelos oculares no tenían simetría rotacional (debido a las topografías personalizadas que se utilizaron).

Los resultados obtenidos fueron resultados de calidad óptica, en términos del error cuadrático medio (RMS) del frente de onda. Estos fueron alimentados en un código personalizado en Matlab (creado por los profesores D. Robert Iskander y Larry Thibos). Este código utilizó los coeficientes de Zernike del software de trazado de rayos para calcular la VSOTF. Esta es una métrica que mide la calidad visual de los modelos simulados del ojo. Esta fue nuestra referencia para comparar la calidad visual de los modelos de los ojos. Los resultados de este estudio proponen que la calidad visual de las LIOs robustas es un poco peor que la de las optimizadas, pero la diferencia no es clínicamente significativa. Esto significa que el paciente nunca observará la diferencia por lo que la optimización no es necesaria. El estudio también mostró que una combinación de dos elementos correctores (LIO y LC) es siempre mejor que un solo elemento de corrección. Por último, los desajustes siempre disminuyen la calidad óptica y visual de los modelos de ojos. La combinación de una LC y un LIO siempre ofrece una mayor tolerancia en los desajustes de la LIO

El quinto capítulo contiene el cuarto estudio de la presente Tesis. Este estudio es una continuación del estudio anterior. Se trata de diseñar LIOs bifocales difractivas en modelos teóricos de ojos humanos personalizados. En concreto, el objetivo principal de este estudio

fue comparar los resultados visuales entre lentes bifocales difractivas optimizadas y robustas (no optimizadas). Las simulaciones contenían tests a distancias lejana y próxima y descentramientos de las LIOs. Al igual que antes, se usó el modelo de ojo de Liou-Brennan. El modelo del ojo fue personalizado alterando la superficie corneal anterior. Se utilizaron datos topográficos corneales retrospectivos de 22 sujetos. Estos datos fueron alimentados en un código personalizado en Matlab, y al procesarse resultaron en coeficientes de Zernike. Estos coeficientes se incluyeron en el software de trazado de rayos con el que diseñamos 22 modelos personalizados de ojo humano. Estos modelos se dividieron en dos grupos diferentes, uno con córneas normales y otro con córneas astigmáticas (astigmatismo corneal mayor de 0,75 D). Se eliminó el cristalino de estos modelos de ojo y se diseñó un espacio vacío en su lugar. A este espacio se le dio el índice de refracción del humor acuoso que normalmente llena este lugar cuando se retira el cristalino. En este espacio se diseñaron las LIOs. Se utilizó un método de diseño específico que añade componentes no secuenciales en el diseño secuencial del sistema óptico para facilitar la desalineación de la LIO posteriormente.

Las LIO difractivas bifocales fueron diseñadas con un código Matlab personalizado (desarrollado por Georgios Zoulinakis). Este código produce un archivo de texto con el diseño de coordenadas para las IOL difractivas. Este archivo de texto se introduce en el software de trazado de rayos, que utiliza las coordenadas para diseñar y simular la LIO. Utilizando los resultados del estudio anterior (capítulo 3), las LIOs diseñadas en este estudio tenían una distribución de potencia superficial anterior del 75% del poder dióptrico total. El patrón de difracción y las asfericidades (segundo y cuarto orden y la constante cónica) fueron diseñadas en la superficie anterior de la LIO. La superficie posterior portaba el resto de la potencia dióptrica de la LIO y la corrección astigmática si era necesaria. Las LIOs optimizadas habían optimizado las potencias dióptricas mientras que los diseños robustos habían escalonado las potencias dióptricas con pasos de 0.25 D. Los desalineamientos de las LIOs incluyen dencentramientos e inclinaciones de las LIOs. Los descentramientos fueron en pasos de 0,25 mm y en magnitud total de 1 mm. Las inclinaciones fueron en pasos de 1 grado y en magnitud total de 5 grados. Todos los desalineamientos mencionados se realizaron en 8 direcciones diferentes. Esto se hizo porque nuestros modelos de ojo no incluyeron simetría rotacional (debido a las topografías personalizadas que se utilizaron). Los datos recogidos fueron en términos de calidad óptica. Esto significa que los resultados

fueron errores de RMS de frente de onda y coeficientes de Zernike de los modelos de ojo con las LIOs. Estos resultados fueron introducidos en un código Matlab personalizado (desarrollados por los profesores D. Robert Iskander y Larry Thibos) que calcula la VSOTF.

Los resultados de este estudio mostraron que la optimización de las LIOs ofrece una mejor calidad visual para ambas distancias pero la diferencia con los diseños robustos no es clínicamente observable. Esto significa que un paciente no percibiría la diferencia entre los dos diseños. La calidad visual para el test de lejos es muy buena mientras que la calidad para el test de cerca es muy pobre. Esto es debido al patrón de difracción que difracta la luz y hace que la imagen final proyectada sea un poco borrosa. Por otro lado, para distancias cercanas generalmente se necesita más luz, lo que resulta en una constricción de la pupila y, posiblemente, una mejor calidad visual. Los desalineamientos disminuyen la visión de lejos mientras que parece que hay un pequeño aumento para la visión cercana. Esto podría cambiar con la restricción de la pupila debido a las condiciones de luz antes mencionadas. Pequeñas magnitudes de desalineamientos podrían ser aceptadas como un resultado final, pero las grandes deben ser corregidas ya que afectan fuertemente la calidad visual final.

El sexto capítulo contiene el quinto y último estudio de la presente Tesis. Este estudio trata sobre la investigación de los sistemas de doble LIO que en realidad conforman un sistema intraocular telescópico (ITS). Estos sistemas son utilizados por sujetos con baja visión, debido a patologías como la degeneración macular asociada a la edad. En estos casos, estas personas pueden utilizar un dispositivo como el que magnifica la imagen observada y proyecta en un área sana de la retina. Este descentramiento de la imagen se realiza descentrando las dos LIOs para que se produzca un efecto prismático. El objetivo principal de este estudio fue diseñar dos tipos diferentes de ITS y comparar los resultados ópticos y visuales. El primer tipo de ITS utiliza una LIO positiva y una LIO negativa con potencias dióptricas diferentes y altas. La LIO positiva se coloca delante de la pupila (cámara anterior) mientras que la LIO negativa detrás de ella (cámara posterior). Así que al final, el ITS se coloca entre la pupila. El segundo tipo de ITS utiliza una LIO positiva y otra negativa de potencias dióptricas iguales y opuestas. Ambas LIOs se colocan detrás de la pupila del modelo del ojo (cámara posterior).

El modelo de ojo Liou-Brennan se implementó en este estudio. Se el eliminó el cristalino del modelo y se dio al espacio vacío el índice de refracción del humor acuoso, que llena este espacio cuando se retira el cristalino. Las lentes fueron diseñadas en ese espacio.

Las LIOs de cada sistema fueron calculadas para tener las potencias exactas necesarias para simular resultados más precisos. Se utilizó un método de diseño que utiliza superficies de rotura de coordenadas con el fin de facilitar el descentramiento de las LIOs. Este es un método diferente al que se utilizó en los capítulos 4 y 5. Ambos ITS fueron diseñados en situaciones optimizadas y no optimizadas. La optimización se refiere a sistemas que han optimizado los términos de 2ª y 4ª asfericidad y la constante cónica en la superficie anterior de la lente positiva para corregir las aberraciones inducidas por la córnea. Los sistemas no optimizados se componían de lentes esféricas sin asfericidades. El descentramiento de las lentes creó un efecto prismático que descentró la imagen proyectada a una posición en la retina que era sana. El descentramiento se realizó en pasos de 0,2 mm y en magnitud total de 1 mm. Se hizo sólo en una dirección ya que el modelo del ojo es simétrico a la rotación. Las simulaciones se realizaron para dos distancias, lejos (infinito) y cerca (~ 40 cm, distancia de lectura cercana). Los resultados de calidad óptica obtenidos fueron evaluados en términos del RMS y coeficientes de Zernike. Estos fueron alimentados en un código personalizado Matlab (desarrollados por los profesores D. Robert Iskander y Larry Thibos) que calcula VSOTF.

Los resultados de este estudio mostraron que los sistemas optimizados (sistemas con asfericidades) proporcionan una mejor calidad óptica y visual como se esperaba. El descentramiento disminuye la calidad visual final pero entre 0,4 y 0,8 mm de descentramiento los resultados no cambian mucho. Este área se propone como un área en la cual los médicos podrían utilizar para descentrar la imagen sin grandes cambios en la calidad de la imagen. Este descentramiento proyectaría la imagen en el área parafoveal. Ambos sistemas ofrecen resultados iguales en términos de calidad óptica y visual para distancias lejanas y cercanas y las diferencias son pequeñas.

En el capítulo final (capítulo 7) se recogen todas las conclusiones finales de la Tesis doctoral actual. También se incluyen algunas ideas para el trabajo futuro en el campo específico de la investigación.

Al final, el apéndice A incluye el código personalizado Matlab creado por Georgios Zoulinakis y una descripción de cómo funciona. Este código se utiliza para diseñar superficies de LIO multifocales difractivas pero también existe la posibilidad de diseñar superficies esféricas o asféricas simples. El código crea en primer lugar una matriz lineal de puntos (pasos), que son las coordenadas radiales de los puntos en la superficie de la LIO. El

número de puntos es proporcionado por el programador. El código crea una función *sag* de difracción con el mismo número de pasos que la línea de matriz creada previamente. El programador en este paso inserta toda la información necesaria sobre la altura del escalón, el factor de apodización, el ancho del patrón de difracción, el número de escalones de difracción y la longitud de onda que está usando en sus simulaciones. También añade la longitud focal cercana que se desea alcanzar con el patrón de difracción. A continuación, el código diseña la función de *aspheric surface sag* que el programador desea aplicar al diseño final. En esta función el programador inserta todos los datos sobre esa superficie. Estos son el radio de curvatura, las asfericidades y la constante cónica. A continuación, el programa calcula todas las coordenadas de los puntos para el caso esférico o asférico. Finalmente, el código aplica el patrón de difracción sobre el *surface sag* y crea la *sag* final de la superficie. La mitad de esta sección se guarda en un archivo de texto en términos de coordenadas de puntos. Este archivo de texto se introduce en el software de trazado de rayos que realiza una revolución de esta media sección alrededor del eje óptico y crea la superficie de la LIO difractiva. Si no se dan datos de difracción en el código de Matlab entonces, se crea una superficie simple asférica (o esférica, dependiendo de los datos). Si esto se utiliza el sofware crea una superficie simple esférica o esférica.

Finalmente, en el apéndice B se incluyen todas las presentaciones y publicaciones que se produjeron a partir de esta Tesis.

Abstract

Correcting elements such as intraocular lenses (IOL) and contact lenses (CL) are commonly used in ophthalmology in order to correct refractive errors, presbyopia and cataract. Thus, these optical elements are in the center of scientific research and development. The optical impact of these elements is the main subject of this Doctoral Thesis. The optical impact refers to the optical results that these elements induce in the optical system of the human eye. The visual impact is also simulated and calculated in order to find the differences between the optical and the visual quality of a human eye model with correcting elements.

Thus, then present Thesis is about developing models using simulations in a computer-programming environment to address the optical and visual impact of optical elements applied in elderly-related disabilities and to propose alternatives to current approaches. All the designs in this Thesis are about IOLs and CLs that are designed following general characteristics and not specific guidelines of a patent or an element that is copyrighted.

In the first chapter, there is a general introduction of the topic. There is information about the human eye biology and its different parts. There is a description of the accommodation function and how is affected by presbyopia. In the end there are listed some methods of correction of the presbyopic effects, such as IOLs and CLs. There is also a short description about the human eye models in general.

In the second chapter, there is a comparative study about human eye models that are used in vision sciences. In this chapter, a comparison between three theoretical eye models is done, the Navarro, the Arizona and the Liou-Brennan eye models. The comparison is about the ability of these models to simulate accommodation and if the results that they produce are the same or if there are differences and where these differences are due to.

In the third chapter, there is a study about the dioptric power distribution between the anterior and posterior surfaces of a monofocal IOL. In this chapter is tested whether the anterior or the posterior surface of an IOL is optimal to carry the largest amount of dioptric power of the IOL. It is also tested on which of the two surfaces the asphericities of an aspheric IOL have to be designed for better optical quality.

In the fourth chapter, a study about optical and visual results is taking place. The study is about monofocal IOLs that are designed in customized (personalized) human eye models. The customization is on the anterior corneal surface that is altered with topographic data from real patients. The IOLs are combined with CLs designs and their designs are either optimized or non-optimized, in order to test the difference between their impacts. There is also a study of different misalignments such as decentrations and tilts, in order to test the tolerance of the designs in such conditions.

In the fifth chapter, there is a continuation of the previous study. Diffractive bifocal IOLs are designed in the same group of personalized human eye models and the optical and visual results are compared. The IOLs are tested without the combination of CLs in this study. There is also a comparison of different misalignments (decentrations and tilts) in order to compare the designs' tolerance in such conditions for far and near target distances.

And finally in the sixth chapter, an intraocular telescopic system is designed with different positioning in the eye model. The position of the telescope changes the optical and visual results produced. There is also a misalignment comparison between the designs that tests the image projection quality on the retinal plane of the model.

Table of Contents

Objective of the Thesis

The aim of this Thesis is to develop theoretical human eye models, with or without optical correcting elements, using simulations in a computer-programming environment. The purpose of this development is to address the optical and visual impact of these optical elements when applied in elderly-related refractive disabilities and to propose alternatives or improvements to current approaches. In order to achieve this, the present Thesis is composed by several chapters of different research studies.

Chapter 1.
Introduction

Human eye anatomy

The eye is the part of the body which provides to human the main sense of perception of his environment, vision. Vision as a sense is the process of image collection and conversion into an appropriate signal which the brain can collect, process and act accordingly to it. This is why our eyes perform two very important functions, the proper focus of images on the photosensitive retina, so that the image is focused sharp and clear and the conversion of light into an electrical signal (electrical impulses) which is transferred through the optical nerve to the brain for further processing.

The eye is positioned into a bony cavity. That cavity is specially configured to offer protection to the eye from external hazards. Provides support to the eye and to the oculomotor muscles, offers enlarged field of vision and a hole for the optic nerve to pass through and travel to the brain. The eye is almost spherical, it has a diameter of about 23-24 mm and the largest portion of it is opaque (about 5/6 of its total area), except from a "window" which allows the entry of light into the eye.[1]

Figure 1.1 *Human eye anatomy. (http://www.eyerisvision.com/anatomy-of-the-eye.html)*

Observing the eye from the exterior layer to the interior the following parts (tunics) are distinguished:

• The sclera, which offers protection and support to the inner parts of the eye so that they are held in place even with the most sudden movements of the eye or vibrations.

• The choroid (or uvea), which is full of blood vessels and provides O2 and other nutrients to the retina.

• The photosensitive retina, which is responsible for the collection of the light and the conversion to a light stimulus (electrical impulse) which is transferred through the optic nerve to the brain.[1]

At the anterior part, the sclera changes its structure and is converted to the cornea. Behind the cornea (in the interior part of the eye) is the iris, the colored part of the eye, which has a hole in the center, the pupil. Behind the iris is the ciliary body and the crystalline lens. [2]

Figure 1.2 *Anatomy of the cornea. (http://www.slideshare.net/NiKeRIO/anatomy-of-cornea)*

• The cornea is the transparent anterior part that allows the light to enter into the eye. It carries the largest portion of the refractive power (~40 to 45 of a total of 60 diopters, D), 2/3 of the total dioptric power of the eye. It has a diameter of 11 to about 12 mm and consists of five distinct layers:

1. Corneal epithelium
2. Bowman's membrane
3. Corneal stroma
4. Descemet's membrane
5. Corneal endothelium

Note that the cornea is avascular and is nourished by the aqueous liquid, which will be commented below.[1, 2]

Figure 1.3 *Anterior part of the eye. Cornea, anterior chamber, iris, posterior chamber and crystalline lens. (http://www.gettyimages.es/detail/v%C3%ADdeo/animation-depicting-a-rotation-of-the-eyes-anterior-pel%C3%ADculas-de-stock/855-114)*

• The iris with the pupil is the natural aperture of the eye. It is part of the choroid and increases or decreases its diameter depending on the lighting conditions. This is done with the radial dilator muscle and the circular sphincter muscle. The iris divides the anterior part of the eye in two parts, the anterior and the posterior chamber. As shown in figure 1.3, the anterior chamber is bounded between the inner surface of the cornea, the anterior surface of the iris and the central portion of the anterior lens capsule. The posterior chamber is bounded by the rear surface of the iris, ciliary body, lateral and posterior capsule and the vitreous.[2]

• The ciliary body extends from the roots (basis) of the iris to the edge of the retina (ora serrata) while the shape of it (sectional cut) is triangular. It is part of the choroid and performs three basic tasks:

1. Accommodation
2. Production and drainage of the aqueous humour
3. Production of the basic components of the vitreous and the Zinn fibers (zonules).

Accommodation is the process that makes clear and sharp the image on the retina as the observed target changes its distance. The ciliary body contributes to this process by its expansion and contraction in order to alter the shape of the crystalline lens. The aqueous humour is the liquid that fills the anterior and posterior chamber. It is responsible for the intraocular pressure (IOP) and provides nutrients to the avascular cornea and crystalline lens.

• The vitreous is transparent, it has a gelatinous texture and fills the space between the crystalline lens and the retina.

• The Zinn zone consists of a set of thin, radially arranged and differentiated collagen fibers (zonules), which start from the epithelium of the ciliary projections of the ciliary body and ends on the capsule of the crystalline lens.[2]

Figure 1.4 *Anatomy of the crystalline lens.*
(http://www.oculist.net/downaton502/prof/ebook/duanes/pages/v8/v8c010.html)

• The crystalline lens is the accommodative part of the eye. It is located between the iris and the vitreous. It is transparent and flexible, linked to the ciliary body with the zonules of Zinn zone and is surrounded by the aqueous humour. The aqueous is responsible for supplying nutrients to the lens. The refractive power of the lens is about 15-20 D and its main role is to focus the image on the retina. This is achieved by altering its shape, which is done with the tensile stress exerted by the ciliary body through the Zinn fibers and thereby changes the dioptric power. Its shape is biconvex and the posterior surface is more curved than the front.[2]

Anatomically the crystalline lens consists of three parts:

1. The capsule. It is a flexible, thick, transparent capsule that surrounds the lens. It is distinguished to the anterior and posterior capsule. The anterior capsule is the base membrane of the epithelium of the lens (lens epithelium).

2. The lens epithelium. It is located in the posterior surface of the anterior lens capsule (inside the lens capsule). The crystalline lens fibers of the main body are born by the lens epithelium. The posterior capsule lacks of epithelium.

3. The main body of the lens. It consists of all lens fibers. The epithelial cells elongate over the years and form the lens fibers, which constitute the essence of the lens. This can be divided in two parts: a) the central core and b) the distal cortex, which surrounds the core.

The cortex of the crystalline lens is composed of many thin layers (such as the interior of an onion), which offers to the lens a gradient (variating) index of refraction along its radius. In the central core the refractive index of the lens is fixed and decreases as the distance from the cortex increase (as we move towards the capsule). This change of the refractive index results in a gradual and continuous refraction of the incoming rays, which reduces the spherical aberration and thus improves the quality of the perceived image by the eye.[2]

Accommodation process

The main role of the crystalline lens is to maintain a sharp and clear image on the retina. Thus, when the eye observes a distant target, the ciliary muscle is relaxed with increased diameter. The Zinn zone fibers are stretched and exert tensile stresses on the capsule of the crystalline lens. The lens is stretched, with reduced thickness and its surfaces (anterior and posterior) are flatter, i.e., with increased radius of curvature. In this geometry the crystalline lens has the smallest dioptric power and focuses on distant targets.[2]

In order to focus on a close target, three different actions happen:

1. Decrease of the pupil diameter.
2. Convergence of the eyes, so that both eyes observe the same target.
3. Focus - Accommodation of the crystalline lens.

The above sequence of actions is called "Triad of near vision".

Figure 1.5 *Accommodation in the normal eye. (https://adithyakiran.wordpress.com/category/eye-health/page/2/)*

Our knowledge about the accommodation mechanism is based on the Helmholtz theory[3]. During the adaptation process, when the eye is needed to focus on a nearby target, the ciliary body is retracted, causes relaxation of Zinn zone fibers. Thus the lens takes its normal shape, which is more spherical. It increases its central thickness, the radii of

curvature of its surfaces reduce and the surfaces become more convex. The anterior surface increases in curvature always more than the posterior (due to the presence of the vitreous). The thickness increase of the lens leads to a reduction in the total dioptric power of the eye. During the accommodation, however the anterior surface of the lens is displaced forwardly (towards the iris). Thus the extra dioptric power generated from the forward movement of the lens and the decrease of the anterior chamber depth (apparently any rearward movement of the lens is prevented by the vitreous). Decrease of the distance between the cornea and the lens leads to an increase in dioptric power resulting from the combination of the corneal and the crystalline lens power. Moreover, as mentioned above, it is possible the distribution of the refractive index of the crystalline lens to contribute to the increase of the total power of the lens when adjusting.[2]

These changes cause the increase of the refractive power of the crystalline lens and of the whole eye.

The mechanism "stimulus - response" that triggers the process of adjustment is not fully understood yet. It is not clear how the human brain understands in what direction will be the change in the refractive index when the eye has a blurred image as a stimulus, although there are signs that in this a leading role have the chromatic aberrations.

While an eye rests, the focal distance is at infinity and the refractive power of the lens is about 19 D. When the eye accommodates to a distance of 10 cm from the anterior surface of the cornea, the refractive power of the lens is about 30 D.[2]

Presbyopia

Presbyopia is the condition in which the eye loses the ability to focus on nearby objects over ageing. It is a condition that starts in the first years of life and progresses, but is perceived in middle age (45-55 years old). The effect of presbyopia makes difficult activities that require close focus (such as reading, computer work, etc.).

***Figure 1.6**. Presbyopia simulation. (http://shapirolaser.com/reading-vision/)*

Myopic eyes have an advantage in terms of presbyopia, as they are already focused on a nearby point when the eye rests. Nearsighted people who have about 2 D of myopia, are

focused at a distance of about 0.5 meters from the cornea. These people do not "feel" the presbyopic effect and are able to see within walking distance simply by removing the visual aids (e.g. glasses).

Presbyopia has become a great field of study and research since the 17th century and until today is an area that attracts the interest of many scientists. This mainly occurs because presbyopia is a condition that advances over time, and everyone sooner or later will feel the effects. So all people over 45 to 50 years old will detect these symptoms, except from myopes as mentioned above, who will feel the symptoms a bit later and in a different way. [4]

There are many theories about presbyopia that have been studied and proposed through years[5] and all of them can be grouped in three main categories:

Lens theories

The lens theories describe all the age changes that affect the lens. As mentioned above during accommodation, the Zinn zonules relax and the elastic lens capsule returns to its normal (and more spherical) shape. It has been observed that crystalline lenses which were extracted in vitro from elderly people, slightly changed their shape in relation to the lenses which were extracted from younger ones, when the capsule was removed. That happened because the lens fibers that were generated by the epithelium superimposed on the former ones, which could not get out from the lens. Thus the increasing population of the fibers fills the volume of the lens capsule. The fibers stick together and create a "hardened core" of the same substance of the lens. The thickness of the lens, its weight and volume increase and the lens becomes more spherical and rigid. There are also other studies[6, 7] which observed that both the elasticity of the lens and its capsule decrease with time. Concluding, lens theories suggest that the highest portion of the reduction of accommodation is due to changes in the elasticity of the lens and the lens capsule.

Out of the lens theories

These theories describe changes that occur outside of the lens. These are age changes that occur in the ciliary body, the Zinn zone, vitreous, iris, choroid and sclera. Many studies have been made to describe these changes, the most important perhaps is the one of

Schachar in 1996[8]. Another theory of presbyopia is based on the alteration of the connection geometry of the Zinn zone fibers with the lens over ageing (known as geometric theory). According to this theory, because of the increased volume (and thickness) of the lens and the front and inward displacement of the ciliary muscle with age, there is a reduced space between the lens and the ciliary muscle. As a result of this, the angle of the fiber connection to the equator of the lens changes. Thus there is a reduced ability of the fibers to exert tensile forces on the lens. This reduction of tension forces lead to increased curvature of the lens and reduces the accommodation. In fact there are no experimental results to support the geometric theory. It has also been shown that changes in the physiology of the ciliary muscle have a very small portion in presbyopia and happen in older people.

Multivariate theories

The so-called multivariate theories combine the aforementioned theories in order to explain presbyopia. However it has not yet been clear whether the changes in the ciliary muscle and lens occur simultaneously or if the ones are the result of the other. In the human eye, the lens loses its elasticity and the movement of the ciliary muscle during accommodation decrease with age. It is possible that the crystalline lens becomes less elastic because the ciliary muscle loses its ability to interact with it. It is also possible that the movement of the ciliary muscle is reduced by the inability of shape alteration of the crystalline lens due to its reduced flexibility. It is also possible that all ageing changes mentioned above occur simultaneously indicating a unified "failure of the accommodation system."

Eventually, evidence up to date show that the primary changes that contribute to presbyopia is the reduction of the elasticity of the crystalline lens and the reduced movement of the ciliary muscle. [4]

Figure 1.7 *Clear and cataractous lens.*
(http://www.drbrendancronin.com.au
/cataracts/)

Cataract

With ageing, the crystalline lens of the eye increases its weight and thickness and the accommodation force is reduced. New layers of lens fibers are added concentrically around the lens cortex, the nucleus of the lens undergoes compression and hardening.

These changes may cause abrupt changes in refractive index of the lens, with effect of light scattering and reduce of lens transparency. The chemical modification of nuclear proteins of the lens increases also the pigmentation, so the lens takes an increasingly yellowish or brownish tint with age. The changes that occur in the lens with age, can affect in the development of cataract, a very common problem of blurred vision in the elderly, the pathogenesis of which is multifactorial and not fully clarified.

This pathology is called cataract and it is a clouding (blurring) of the lens, which often happens with age.[2]

Addressing presbyopia

Whilst presbyopia is a pathology that eventually affects all people, there are many different ways and procedures that have been developed in order to address it. It should be noted though, that all procedures and remedies up to today, address to the refractive error that is the result of presbyopia and not to presbyopia as a pathology. Unfortunately, up to date there is no method to prevent the progression of presbyopia.

Below there is a report of some popular and state of the art ways to address the errors that are caused by presbyopia. There is a short description of them and a more detailed one for the main elements that were used in this work: the intraocular lenses (IOLs) and the contact lenses (CLs).

Spectacle lenses – Lenses that are designed and manufactured to be placed on spectacles.

Monovision – A situation where the primary eye is fixed to be focused at far distance while the secondary is fixed to be focused at a reading distance.[9]

PresbyLasik – Surgical procedure with Excimer Laser that designs a (refractive) multifocal lens on the cornea of the patient.[10]

IntraCOR – Intrastromal presbyopia correction, a surgical procedure with Femtosecond Laser that creates concentric circle cuts in the corneal stroma. The cornea relaxes and is pushed outwards by the IOP, creating a myopic condition in the eye which focuses at a close distance.[11]

Corneal Inlays – Inlays, either refractive (lenses) or diffractive (pinhole apertures) that are placed in the corneal stroma and create either a multifocal effect or an extended depth of focus (because of the pinhole effect) respectively.[12]

Contact Lenses (CL)

CLs are widely used from people that face refractive errors and they don't want to use their spectacles. There are different types of CLs (rigid, soft, monofocal, multifocal etc.) between a variety of companies, materials and types in order to fit every single person. There are also CLs for short-term use (daily, 3 days, weekly) or for longer periods (monthly or yearly). There is a large industry and research field that support the safe use of them and in the last years there is a lot of research still going on to improve them even more.

Figure 1.8 *Contact lenses. (http://owensoptometrics.com/contact-lens-exams.html)*

CLs are used from presbyopic people too. These can be either monofocal lenses both of the same power, so the patient uses them for one distance and needs another correction (such as spectacles) for another distance. The monofocal lenses can be chosen to be of different powers so that a monovision situation is triggered.

Multifocal CLs are also common for presbyopic people. These lenses have concentric regions of different dioptric power and the patient focuses on different distances by the pupil diameter changing.[13]

Intraocular lenses (IOL)

IOLs were created in order to replace the crystalline lens when it has to be removed. This procedure has to be done in cases of cataract, presbyopia or other reasons. The main characteristic of these lenses is the high dioptric power that they provide to the eye (about 20 - 25 D or even more) in order to correct the hyperopia that is created by the lens removal.

Figure 1.9 *Different types of intraocular lenses.*
(https://www.doctor-hill.com/iol-main/polypseudophakia.html)

There is a large variety of IOLs: monofocal, bifocal, multifocal, adaptive IOLs of different types of polymeric materials and silicones. The research field behind these lenses is huge and multiscientific: medical doctors, optometrists, physicists, mathematicians, engineers and optical designers work together in order to make these lenses better.

Figure 1.10 *Folded IOL through syringe.*
(http://www.stansholik.com/intraocular-lenses.htm)

The insertion process is done through a small incision through the cornea. Through the incision the doctor performs a rupture of the anterior lens capsule (anterior capsulorhexis) and divides the lens into small pieces using ultrasounds. Then, the lens pieces are sucked out by a vacuum device and the insertion of the IOL is done through a specific syringe, which imports the IOL folded. After the IOL is placed in the lens capsule, it unfolds to its normal shape. Lately, the incision at the cornea and the division of the crystalline lens is performed using Femtosecond Laser technology which offers greater accuracy and comfort throughout the surgical procedure.[14]

Eye models for simulations

In this work all the studies are about simulations. In order to simulate optical and visual results in human eyes an optical designing program was implemented. In this program, different theoretical eye models were designed and used.

Theoretical eye models are a tool that represents the human eye by using mean values for the parameters of their designs (radius of curvature, refractive indices, thicknesses etc.). These mean values come from studies all around the world that have measurements from human eyes.

The eye models can be divided in many categories.[15] There can be categories like reduced or anatomical (depending on the number of surfaces that they use), monochromatic or polychromatic (depending on the refractive index dispersion), with homogeneous or gradient index crystalline lens, unaccommodated or accommodative, age-independent or aging and many more.

In this work three different eye models were used. The Navarro eye model[16], the Liou-Brennan[17] and the Arizona[18].

In figure 1.11 there is a human eye model in an optical design program.

(figure available in printed version)

Figure 1.11 *Human eye model, (1) cornea, (2) anterior chamber, (3) pupil, (4) posterior chamber depth, (5) crystalline lens, (6) vitreous, (7) retina.*

In this figure are obvious the different parts of the eye model which in the optical program are considered to be lenses. So in the end, an eye model is a composition of different lenses placed one after the other, in order to compose the final optical system. In figure 1.11 the anterior chamber (2), the posterior chamber (4) and the vitreous (6) have the same colour because they have almost the same refractive index (1.336). In the same figure the cornea (1) and the crystalline lens (2) have the same colour because the cornea has a refractive index of 1.376 while the crystalline lens has a refractive index between 1.368 in the periphery and 1.407 in the center (gradient index).

In figure 1.12 there is a human eye model with a CL and an IOL in the position of the crystalline lens.

(figure available in printed version)

Figure 1.12 *Human eye model, (CL) contact lens, (1) cornea, (2) anterior chamber, (IOL) intraocular lens, (3) posterior chamber, (4) vitreous, (5) retina.*

In this figure the IOL is placed in the posterior chamber (in the crystalline lens capsule) and the whole space has the same refractive index of the anterior chamber (1.336) as it is filled with the aqueous humour that fills both the anterior and posterior chambers.

Chapter 2.
Eye models used in optical design

Introduction

Optical modelling of the human eye is a field with a large variety of models, either new or alterations of old ones [15, 18]. There has also been research in trying to create an eye model to fit the statistical data collected from healthy people[19]. In the end there is no model that could be widely used in the visual research field. All of them use almost the same parameters, based on the way that they are designed (e.g. mean parameter values based on population, optimized parameters for specific results etc.). Differences between simple and more complicated designs (with three or four refractive surfaces) exist, depending on the reason for which they are used. Some models are designed either with a simple crystalline lens, or with grading refractive index or even with an accommodating crystalline lens. Each model has advantages and disadvantages, can simulate different procedures, parameters and metrics of the human eye[15, 20].

Nevertheless, there is still need for more eye models in order to cover different areas of research such as ray-tracing of non-symmetric eye models[21] and models with missaligned optical designs[22]. Further investigation and comparisson studies are held and needed because the natural human eye has a robust optical design which differs between people[23].

In this work three different models were used: the Navarro model[15, 16], the Arizona model[18], which is accommodating by using mathematical functions and the Liou-Brennan[17], which is a more anatomically accurate model.

The Navarro model[16], was firstly created in 1985 and consists out of four centered aspheric refracting surfaces. Each one of them represents a refracting surface of the human eye: two for the cornea and two for the crystalline lens. It also uses a flat retinal surface, although there are also versions with spherical retinal surface as well. The main characteristic of this model is that it has a flat surface as a retina. This makes it suitable for on axis simulations. As rays create an angle in respect to the optical axis the image gets defocused and the coma aberration increases. The other models use a spherical surface for the retina. It is a simple model with rotational symmetry, axial length 24 mm and a total dioptric power of 60.4 D.

The Arizona model[18], is also rotationally symmetric. It has the ability to accommodate in different distances by altering its dioptric power. This is done by use of mathematical

functions that change the geometry of the crystalline lens, its refractive index and the anterior chamber depth. In this way it can simulate every particular change of its media during the accommodation process. Its axial length is 24.003 mm but the total dioptric power depends on the accommodation distance.

A more anatomically accurate model was created by H. Liou and N. Brennan in 1997[15, 17]. Its major difference is that it has a gradient refractive index for the crystalline lens instead of a simple one. It is not rotationally symmetric because of the decentration of the pupil by 0.5 mm nasally. This decentration affects aberrations, particularly coma, as well as curvature of field and vignetting. The equivalent power of this model is 60.35 D and its axial length 23.95 mm.

There are accommodative models in our knowledge such as the Arizona that can accommodate by their own and even simulate the ageing of the eye[24]. There are also computer animated models that show how the parts of the eye move with accommodation and studies about the changes in the crystalline lens with ageing and the mechanisms of accommodation[25-30].

In our work the accommodation function in accommodative and non-accommodative models is examined and compared. The Arizona model is able to accommodate by the use of mathematical equations for its media. The other two models were designed to be non-accommodative. Values chosen from the literature were inserted in order to simulate accommodation[31]. This comparison study will provide us knowledge on simulation of accommodation with different customized models.

Comparing to previous works mentioned above, in this study we compare one accommodative and two non-accommodative models. The main target is to check if non-accommodative models can provide simulations of accommodation. Moreover, there is a comparison with an accommodative model in order to compare the results between them.

Methods

Ray tracing software package (Zemax, USA) was implemented to design and work with the eye models. The models were chosen because they are mostly used in modelling of vision science research. The common feature of the chosen models is that all of them have

aspheric refractive surfaces. On the contrary, they use different parameters for simulating the optical procedure of the human eye. These differences are between the retinal surfaces, optical and visual axis, types of crystalline lenses and values for their optical media.

All models that were used in this study were designed following the works published by their designers[16-18]. They have four refractive surfaces, two for the cornea and another two for the crystalline lens. In the Liou-Brennan model the crystalline lens has a grading refractive index and was designed by two different parts, one for the anterior part of the lens and one for the posterior. The refractive indices and the thicknesses of all the media were taken from the original articles.

In the following part of the methods, all tools and terms concerning the ray tracing sofware will be written in *Italics* for clarity.

Accommodation in human eye models

All previously described models are designed to be non-accommodative, except from the Arizona. The other two models are fixed to focus at infinity, while the Arizona model can focus at any accommodative demand by using the mathematical algorithms that come with it. In order to compare accommodation results between these models, the Navarro and Liou-Brennan models had to accommodate as well.

Four different target distances were used to simulate the accommodation process. These were for infinity, 3 m, 1 m and 0.5 m (0 D, 0.3 D, 1 D and 2 D accommodative demand in respect). Each chosen value of change corresponds to a specific accommodative demand. The target distances were introduced in the sofware in the *Thickness* box of the *Object* line and the units used were mm (millimeters). For these simulations two fields of incoming rays were used, parallel to the optical axis (0 degrees angle) and not parallel (5 degrees angle). These were introduced in the *Field Data Editor* in the ray tracing sofware. The wavelength that was used was 587.6 nm, which is the middle one of the *F, d, C (Visible)* wavelength group in the *Wavelength Data Editor.*

In every distance all models were optimized. That was done because of changing their parameters (radii of curvature of the lens, thicknesses of their media etc. as it will be explained in the following paragraphs) in order to accommodate. The models had to be optimized in order to create a clear image on the retina with the given parameters and to compare their results. This optimization was done with the *Optimization Tool* of the ray

tracing sofware. This uses a *merit function* that minimizes the root mean square (RMS) error in the retinal plane and is defined as $MF^2 = \frac{\sum W_i (V_i - T_i)^2}{\sum W_i}$, where MF is the merit function value, W is the weight factor for each operand used for the calculation of the merit function value, V is the value of each operand, T is the target value for each operand and the factor "i" is for all the population of the operands. The ray tracing sofware took into account the variable that was chosen and made all the calculations in order to minimize the merit function value. In the end it returned the best value of the chosen variable.

For the optimizations in this study a *Default Merit Function* was implemented to calculate the least RMS wavefront error in the centroid of the image created in the retina. In the *Pupil Integration Method,* 3 rings and 6 arms of incoming rays was used in a *Gaussian Quadrature.*

As an optimization variable was selected the vitreous thickness. That was done because this was the only free parameter while the model was getting optimized. During accommodation the corneal parameters (curvatures and thicknesses) and refractive indices of all media do not change. The anterior chamber depth, the crystalline lens thickness and the curvatures of the crystalline lens surfaces are changing and set by us.

While simulating accommodation by changing the target distances and the parameters mentioned above, if the chosen values for the parameters are not suitable, then there will be an obvious change in the total length of the eye. This change will occur through the optimization process which will try to minimize the RMS wavefront error in the retina by changing only the vitreous thickness.

The changes of the ocular system during accommodation are known and studied thoroughly before. All these changes happen with a small increase in the total length of the eye[31-37].

In order to make the Navarro and Liou-Brennan models to accommodate, specific values from the literature were used[31].

While accommodating the anterior chamber depth decreases and the crystalline lens thickness increases. The crystalline lens changes it's shape to become more spherical by decreasing it's radii of curvature. The pupil diameter also decrease in order to increase the depth of focus.

The refractive index of the crystalline lens naturally is gradient. This means that its dioptric power depends on the geometrical characteristics of the lens. There are two ways to simulate this dependency: either to change only the geometrical characteristics (Navarro and Liou-Brennan models) or to change the refractive index of the lens too (Arizona model).

The parameters that were changed during accommodation were: the anterior chamber depth between 3.35 mm and 3.23 mm, lens thickness between 3.85 mm and 4.03 mm (corresponding *Thickness* box of each line), anterior radius of curvature of the crystalline lens between 12.8 and 11.5 mm and posterior radius between 5.96 and 5.22 mm (corresponding *Radius* box of each line). The pupil radius also changed from 2 mm to 1.5 mm (corresponding *Semi-Diameter* box of each line). These changes occur while the target comes closer to the model. All values were chosen as mean values of parameter changes in order to accommodate, following the concept that all eye models are designed with mean values of real human eyes.

The Arizona model has an algorithm that makes it accommodative[18]. In this way is optimized in all distances. The algorithm has mathematical functions that change the geometrical characteristics of the crystalline lens and the aqueous thickness. The refractive index of the crystalline lens in this model also changes while accommodating. This happens because in this model a simple refractive index is used. The physiological refractive index is gradient and while accommodating is dependent on the geometric characteristics of the crystalline lens. In order to simulate this change, this model slightly changes the index while it accommodates.

In this model the same values were used as in the Navarro. The difference here is the procedure of changing the thickness of the lens. In this model the crystalline lens is divided in two parts with different thicknesses and with a grading refractive index. In order to set the crystalline lens thickness, firstly the total thickness of the unaccommodated lens (in 0 D) was subtracted from the needed in each accommodation level. The result was divided by 2, and each half was added to each of the parts. In other words, it was assumed that the two parts change their thickness equally while accommodating.

Results

In the following results “non-optimized” refers to each model coming from the literature, without any optimization. “Optimized” refers to each model after the optimization process that was mentioned earlier.

For graphical comparison, image diffraction analysis was used. In figure 2.1 there is a comparison between letter F diffraction images from each model at all distances. As expected, the image gets clearer as the target approaches to the model. Moreover, in Navarro and Liou-Brennan models are obvious the differences between optimized and non-optimized results at infinity.

(figure available in printed version)

Figure 2.1 *Letter F diffraction images. In this figure are shown the images of a letter F as they are simulated in the retinal plane of the eye models in each target distance. The Arizona model is optimized in all distances, as an accommodative model.*

Spot diagrams show the intersection of a ray pattern with the retinal field. Modulation Transfer Function (MTF) diagrams show the response of the models in each accommodative level, between 0 and 100 cycles/mm.

In figure 2.2 the differences between optimized and non-optimized models at infinity are more obvious in the Navarro model. In both models, optimized spot diagrams are smaller from the non-optimised ones and the MTF diagrams show better results for the middle spatial frequencies.

(figure available in printed version)

Figure 2.2 *Differences between optimized and non-optimized models at infinity. In spot diagrams the dimension is in μm. In modulation transfer function (MTF) diagrams the dashed line shows the diffraction limit for a pupil radius of 2 mm. The double line in the Liou-Brennan MTF diagrams is because of the decentration of the pupil.*

In figure 2.3 are shown the spot diagrams for three different target distances. It is obvious that the diameter decreases as the target approaches the models. In Liou-Brennan model, the decentration of the pupil creates a “tail” in the spot diagrams (coma aberration).

(figure available in printed version)

Figure 2.3 *Spot diagrams for the three eye models. In the Liou-Brennan model the circles of the rays are decentered to the right of the central spot because of the decentration of the pupil, creating the characteristic tail of the coma aberration. All dimensions are in μm. In each of the spot diagrams the left one is for 0 angle and the right one for 5 of angle between the incoming light rays and the optical axis.*

In figure 2.4 the MTF diagrams show again better results as the target distance decreases, which is expected. In the Arizona model the results are almost diffraction limited. This model is designed to have the best results as a perfect optical system that simulates a real eye. The diffraction limit decrease in the figures, as the target distance decrease. That happens because of the decrease of the pupil.

(figure available in printed version)

Figure 2.4 *Modulation transfer function (MTF) graphs for the three models. The dashed line shows the diffraction limit. (OTF: Optical Transfer Function).*

The total eye lengths of the optimized Navarro and Liou-Brennan models are shown in Table 2.1. It is obvious that both models change their total length while accommodating. The Navarro model shows smaller difference in its width than the Liou-Brennan. These total lengths are different from the ones that were mentioned earlier and that's because of the optimization method that was applied.

Table 2.1. *Total eye lengths. Total eye lengths for the optimized Navarro and Liou-Brennan models. The Arizona model does not change its length while accommodating.*

Distance of target (m)	Infinity	3.0	1.0	0.5
Accommodative level (D)	0.00	0.33	1.00	2.00
Navarro total length (mm)	24.27	24.33	24.39	24.48
Liou-Brennan total length (mm)	23.70	23.79	23.95	24.15

Zernike coefficients of defocus and spherical aberration, both primary and secondary are shown in Table 2.2. In the Navarro and Liou-Brennan models are obvious the differences before and after optimization at infinity. All models decrease their aberrations as the target approaches, as a result of the pupil diameter decrease and the aberrations that are introduced by the crystalline lens.

Table 2.2. *Zernike coefficients. The Zernike coefficients for the eye models in all distances of accommodation.*

		Distance	Pupil diameter (mm)	Defocus (nm)	Spherical Aberration (nm)	Secondary Spherical Aberration (nm)
Navarro model	Non-optimized	Infinity	4.0	382.6	69.9	0.8
	Optimized	Infinity	4.0	-77.3	89.3	0.5
		3.0 m	3.6	-62.3	59.4	0.3
		1.0 m	3.2	-49.0	38.1	0.2
		0.5 m	3.0	-42.8	31.1	0.1
Arizona model	Optimized	Infinity	4.0	74.9	17.8	0.2
		3.0 m	3.6	68.7	16.3	0.2
		1.0 m	3.2	55.7	12.9	0.2
		0.5 m	3.0	33.7	6.6	0.2
Liou-Brennan model	Non-optimized	Infinity	4.0	162.4	32.3	-0.4
	Optimized	Infinity	4.0	103.5	72.1	1.1
		3.0 m	3.6	86.8	49.7	0.6
		1.0 m	3.2	75.0	34.4	0.4
		0.5 m	3.0	75.6	31.4	0.5

The RMS diameter is the root-mean-square error radial size. It is a rough image of the spread of rays on the retinal field. The Airy disk diameter shows the diameter of the light spot focused on the retina and depends on the diffraction of light through the pupil and its diameter[38, 39].

In Table 2.3 are included the RMS error and Airy disk diameters of the eye models while the target distance decreases (and the models accommodate). The results of Table 2.3 are graphically presented in figures 2.5 and 2.6.

Table 2.3. *Root-mean-square (RMS) error radius and Airy disk diameter. RMS radius and Airy disk diameter for all eye models in all distances of accommodation.*

		Navarro model	Arizona model	Liou-Brennan model
Non-optimized Infinity	RMS radius (μm)	21.5		3.5
	Airy diameter (μm)	5.2		8.4
Optimized Infinity	RMS radius (μm)	8.4	6.2	15.9
	Airy diameter (μm)	5.2	7.0	5.1
Optimized 3 m	RMS radius (μm)	5.9	5.7	13.2
	Airy diameter (μm)	5.8	7.0	5.7
Optimized 1 m	RMS radius (μm)	4.1	4.6	11.4
	Airy diameter (μm)	6.6	7.0	6.5
Optimized 0.5 m	RMS radius (μm)	3.5	2.6	11.8
	Airy diameter (μm)	7.0	7.0	7.0

Obviously, the RMS error diameter decrease as the model eye accommodates and the Airy disk diameter increase as the pupil diameter decrease.

(figure available in printed version)

Figure 2.5 *Root-mean-square (RMS) error radius over target distance.*

(figure available in printed version)

Figure 2.6 *Airy disk diameter over target distance.*

Discussion

In the present study there has been a comparison between three schematic eye models (Navarro, Arizona and Liou-Brennan)[16-18] in terms of accommodation. The Arizona eye model was able to accommodate by a mathematical algorithm while the other two models had to be changed. These changes included alterations of the radii of curvature of their crystalline lens and the thicknesses of the anterior chamber and the crystalline lens, as

the target distance was decreasing. All the parameter changes were selected from the literature. An optimization was implemented in the models with variable the vitreous thickness, in order to get the best image quality in the retina with the chosen parameters in each target distance. A successful accommodation should result in small or no change at all in the vitreous thickness (and the total eye length), while a failure in accommodation should result in unrealistic changes in the total eye length (e.g. larger than 1 mm).

Letter F diffraction images

From figure 2.1 is obvious that the optical result on the retina is optimal for all models while accommodating. The Navarro model is a bit myopic, as it is obvious for the far target distances but the image gets clearer as the target distance decrease. The Liou-Brennan model has a characteristic coma blur at the right of the image. The Arizona model shows almost the same retinal image for all distances because it is created to be always optimized through mathematical functions. It doesn't simulate an average eye but a perfect one. All our results and images are optical simulations of the image as it is refracted on the retina. For the visual results, the neural process that takes place in the brain has to be taken into account, which is not a topic of this paper.

Spot diagrams and MTF graphs

In figure 2.2 and 2.3 the comparison shows that the best accommodation is given by the Arizona model. On the other hand, the other two models show quite similar results and in a good accordance to the Arizona. Moreover, the Liou-Brennan model also simulates the characteristic coma "tail" which is a result of the decentration of its pupil.

In figure 2.4 the Arizona model shows a better MTF than the other models and is close to be diffraction limited. But it is known that the real eye is far from that.

Total eye lengths

While accommodating both the Navarro and Liou-Brennan models change their total length while the Arizona model is not. The changes between the accommodation levels are small and comparable between them. Our simulations' results are in the same way with some new studies that have measured the axial length in vivo[32, 40], but the difference

between our results and theirs is about one magnitude class. This difference is assumed to exist because in our work a merit function was used in order to optimize our models. So there has to be a difference between the merit function of the optical design program and the one that a real human optical system uses.

Aberrations

In the aberration results the Navarro model shows a negative sphere coefficient while the other two models have a positive one. This negative sphere results in a blurry image. All models also have a positive spherical aberration while the secondary spherical aberration is almost zero. It can be observed that the sphere and spherical aberration increase or decrease (in absolute values) in parallel. In other words, the spherical aberration always tries to correct the total sphere that is produced by the cornea and the accommodation process.

According to our results we have observed that the non-accommodative eye models can simulate accommodation if they are fed with sufficient and correct data. To our knowledge there in no study to compare our findings with, but there exists a work in comparing non accommodative eye models[41]. If we compare our findings with this study, then we have to agree that the Liou-Brennan model is more accurate to the biological human eye. It is more detailed by using a gradient refractive index lens and a decentred pupil but this does not make it the perfect model. If this model is selected to simulate a real human eye then more data are needed to be input, in order to be more accurate. There is no model eye that we can propose as the best and the selection depends always on the study, the data that are used and the complexity of the model that is needed.

In the field of the vison science there are many works about accommodating eye models, theoretical and computer designed[24-31] and about how they are created or designed to work. In this study it is shown that, the classical models, even the ones that are not designed to simulate accommodation could be possible tools in research. If they are fed with data that optimize accommodation they can provide simulations which are comparable with the ones of accommodating eye models. So, in a possible input of customized data from a specific subject, they should be able to simulate this customized eye as well. These simulations could be a first tool in simulating far and near vision for specific applications like spectacle or CLs design or fitting. They can also provide some results for blurred vision,

halos, lightscattering, loss of contrast sensitivity etc. It has to be noted that these can be only the first results, and further research, tests and analysis should be considered.

We can conclude that the three models simulated accommodation in good accordance compared between each other. Every difference between the simulations' results, can be changed by changing the parameters of their optical media. Providing them with more accurate values, we can customize them and get more precise results, maybe without differences between models.

Chapter 3.
Power distribution in monofocal spherical and aspherical intraocular lenses

Introduction

As people grow older, different problems appear in their visual system. Two common pathologies are presbyopia and cataract. These two problems affect the crystalline lens and the refractive part of vision. In presbyopia the crystalline lens gets stiffer and thicker and it loses the ability to accommodate on near targets. Cataract makes the crystalline lens blurry and scatters the light to every direction, making the final image blurry with low contrast.[4, 6, 7, 34, 42]

In order to compensate these problems, a common practice is to remove the crystalline lens and change it with an IOL.[14, 43] There is a large variety of IOLs in the market with different materials and designs. There are monofocal IOLs with only one focus in one target distance or multifocal with 2 or 3 foci and a depth of focus depending on them.[44-46] Multifocality is designed with different ways, either with refractive zones or with diffractive patterns. There are also models that claim to be accommodative and change their focus by moving their optical elements.

The field of the IOLs is growing and there is a lot of research being carried on about their designs and the results that different IOLs offer and how to predict and calculate the results.[47, 48] In this project the main purpose is to find out which would be the optimal power distribution between the surfaces of an IOL. Would it be better to have more power on the anterior or the posterior surface of the IOL? After answering that question, the next step would be to find out which would be the optimal choice to design the asphericities, either on the anterior or posterior surface of an IOL.

In the end, the main purpose of this study was to find out which would be the optimal design of a monofocal lens when it has spherical or aspheric surfaces, in order to provide better optical results.

Methods

In this project an optical design program[49] was implemented in order to design the human eye model and the IOL that were used. There are other optical designing programs

in our knowledge that could be used as well, but this one was available in our lab and we were able to use it.

A central field of incoming light rays was used of a single wavelength of 555 nm (green light, monochromatic). The field of rays was parallel to the optical axis of the eye model (0 degrees of inclination) and it was filing the whole pupil area (pupil diameter 3 mm).

The Navarro eye model[16] was implemented for this study. There are more complicated and new eye models in our knowledge that could be used.[15] This was chosen specifically because there was the need of a simple eye model for our research. In any case, more complicated models are used in order to describe differences in the crystalline lens, such as gradient refractive index models etc. In this particular study, the crystalline lens is missing because it has been exchanged with an IOL, so there is no need of another model. Nevertheless, it is expected that a more complicated one could provide more information if we needed to make a more detailed or personalized (customized) study based on patient measurements.

Two different types of projects were done in this study, both of them based on designing IOLs with different parameters. The first one was about the power distribution of the total dioptric power of the lens between its two surfaces. The second one was, after finding the best power distribution, to test on which of the two surfaces (anterior or posterior) would be better to place the asphericities and conics in order to get better optical results.

All lenses designed in this project, were designed for far vision (>6 m target distance). They do not represent any patent or specific material used in practice. They were designed for research reasons only.

Power distribution on spherical lenses

For this project 5 different IOLs were designed with total dioptric powers of -10, 10, 20, 30 and 40 D. The common characteristics of these lenses were the refractive index that was set at 1.55, their diameter that was 6 mm and their central thickness that was 1 mm. All of them were designed behind the pupil at a distance of 1 mm from it. Their surfaces were spherical, with no asphericities designed for this project.

For each of these lenses 5 different designs were implemented. Each design had to do with a different power distribution between the anterior and the posterior surfaces of the

lens. The designs were of 0%, 25%, 50%, 75% and 100% of the total dioptric power on the anterior surface of the lens, where the 0% is a plano-convex lens and the 100% is a convex-plano lens (figure 3.1).

(figure available in printed version)

Figure 3.1 *Lenses with equal power and different power distribution between its surfaces.*

For designing the different IOL surfaces in the optical design program we needed to calculate each surface radius of curvature. The radius of curvature for each surface of the lens was calculated by the formula of surface dioptric power

$$R = \frac{n_2 - n_1}{P},$$

where R is the radius of curvature of the surface, P is the proportion of the power of the surface and $n_2 - n_1$ is the difference between the refractive indices of the IOL and the aqueous humor. For the anterior surface of the lens, n_1 is the IOL index and n_2 is the aqueous index (1.337). For the posterior surface of the IOL n_1 and n_2 are the opposite.

When the design of each lens was done, the next step was to optimize each eye model with this particular lens. The main purpose of this was that we wanted to observe the difference between the optical impact (optical result) of these lenses, taking into account that they were perfectly designed for each eye model and compare their differences, if there were any. For example, we wanted to test if there are any differences in the optical result of an IOL of 30 D with different power distribution between its surfaces, if this lens is ideal (in terms of dioptric power) for an eye model.

The optimization process was done with the optimization tool of the ray tracing sofware. This tool uses a merit function that can be selected by default through the program. This function is minimizing the wavefront RMS error by altering the variables that are chosen by the programmer. In this case the only variable that we chose to be changed was the vitreous thickness, so the program actually changed the vitreous thickness of each eye model so that the lens of each power was ideal for each eye model. So in the end the only parameter that could change the results of each IOL was the power distribution between its surfaces.

IOL surface asphericities

In the second project of this study, we used the result of the first study. After finding the best proportion of power distribution for each lens, the question was on which surface would be better to design the asphericities in such a lens. In order to observe this, we used the same eye model, IOL designs and vitreous thicknesses from the previous project. There were two main differences.

The first was the pupil diameter. In this project the pupil diameter was at 6 mm instead of 3 mm, as it was on the previous project. That was selected in order to observe what happens in eyes that use a larger pupil diameter, because it is known that as the pupil gets smaller, the optical results get better (smaller area of the refractive means is used so less aberrations are induced to the final result).

The second difference was that there was a second optimization, this time on the lens. Either if the asphericities were designed on the anterior or posterior surface, these were optimized so that the lens was specifically designed for each eye model. So, for the same IOL power, the only parameter that could induce a difference in the optical results was the selection of the anterior or the posterior surface to carry the asphericities.

Each IOL surface in this project was designed by the asphere surface sag formula:

$$z = \frac{cr^2}{1+\sqrt{1-(1+k)c^2r^2}} + a_1 r^2,$$

where z is each surface point height, $c = \frac{1}{R}$ is the curvature of the surface and R is the radius of curvature, k is the conic constant of the surface, r is the radial coordinate of each point and a_1 is the 2nd order aspheric constant.

In the second optimization procedure, k and a_1 were selected as variables for optimizing the IOL. After the optimizations for each project there was done a ray tracing and the optical results were collected.

Results

Our results were collected after the ray tracing procedure that was done from the optical design program. These included the wavefront RMS radius (in μm) and the geometrical radius (in μm) on the retina of each model, the total wavefront RMS error (in

nm) and the Zernike coefficients (in nm) for both projects. The geometrical radius refers on the total radius of the spot that is projected on the retina while the wavefront RMS radius is the radius of the main spot from which the RMS is calculated.

Power distribution on spherical lenses

For the first project of this study the results we collected are shown in table 3.1. The results are grouped per lens total dioptric power and for each power distribution. In the following table we did not include the sphere and secondary spherical aberration because they were very small (less than 0.5 nm) compared to the rest of the spherical aberration.

Table 3.1 *Results for IOLs with different total dioptric power and power distribution between surfaces.*

Anterior surface power portion	0%	25%	50%	75%	100%
IOL total power (D)	-10				
Total wavefront RMS error (nm)	29.3	28.6	27.5	26.1	24.4
Spherical aberration (nm)	29.7	28.9	27.8	26.4	24.7
RMS radius (µm)	7.752	7.570	7.305	6.952	6.508
Geo radius (µm)	13.606	13.287	12.821	12.202	11.422
IOL total power (D)	10				
Total wavefront RMS error (nm)	36.6	34.9	33.4	32.2	31.3
Spherical aberration (nm)	37.1	35.3	33.8	32.6	31.6
RMS radius (µm)	6.576	6.255	5.982	5.758	5.582
Geo radius (µm)	11.544	10.979	10.501	10.108	9.799
IOL total power (D)	20				
Total wavefront RMS error (nm)	56.0	46.5	39.5	34.7	32.3
Spherical aberration (nm)	56.6	47.1	39.9	35.1	32.6
RMS radius (µm)	8.676	7.190	6.085	5.339	4.940
Geo radius (µm)	15.238	12.625	10.683	9.373	8.672
IOL total power (D)	30				
Total wavefront RMS error (nm)	95.8	68.4	50.0	39.6	37.1
Spherical aberration (nm)	97.0	69.3	50.6	40.1	37.5
RMS radius (µm)	13.108	9.323	6.776	5.342	4.965
Geo radius (µm)	23.053	16.382	11.899	9.379	8.714
IOL total power (D)	40				
Total wavefront RMS error (nm)	165.6	104.7	66.8	49.0	50.2
Spherical aberration (nm)	167.5	105.9	67.6	49.6	50.8
RMS radius (µm)	20.346	12.779	8.095	5.880	5.960
Geo radius (µm)	35.857	22.480	14.223	10.324	10.463

These results could be graphically shown in the next figures.

(figure available in printed version)

Figure 3.2 *Wavefront RMS and geometrical radius.*

In figure 3.2 are graphically shown the RMS radius and the geometrical radius of the eye models with each lens and for each power distribution.

(figure available in printed version)

Figure 3.3 *Total wavefront RMS error and spherical aberration coefficient.*

In figure 3.3 are graphically shown the total wavefront RMS error and the spherical aberration coefficient of the eye models with each lens and for each power distribution. It could be observed that a power distribution of ~75% of the total dioptric power of the IOL should be on the anterior surface of the IOL, especially for IOLs with high dioptric power (e.g 30 or 40 D).

IOL surface asphericities

In table 3.2 are shown all the collected results for the wavefront RMS error and the coefficients for sphere, spherical aberration and secondary spherical aberration for the second project of this study. The results are grouped per IOL power, for the anterior and the posterior surface asphericities and for power distribution of 70%, 75% and 80% of the total dioptric power on the anterior surface of the lens. The comparison between these distributions was done in order to compare and find out the potentially optimum power distribution in addition to the asphericities designed on the lens (either on the anterior or the posterior surface).

Table 3.2 *Optical quality results for asphericities designed either on the anterior or the posterior surface of the IOL. (*Secondary spherical aberration)*

Asphericities	Anterior surface			Posterior surface		
Power Distribution	70%	75%	80%	70%	75%	80%
IOL power (D)	-10					
RMS (nm)	44.3	41.0	38.2	101.3	123.8	119.0
Sphere (nm)	-1.0	-0.9	-0.7	-8.2	-13.2	-43.1
Spherical aberration (nm)	-7.0	-6.2	-5.5	-28.0	-38.5	30.0
Secondary Sph. Aber. (nm)*	-44.5	-41.3	-38.5	-97.2	-116.1	-103.2
IOL power (D)	10					
RMS (nm)	133.7	126.5	132.2	371.5	401.0	430.9
Sphere (nm)	7.3	8.2	9.0	-2.2	-3.0	-3.8
Spherical aberration (nm)	69.4	29.0	-11.2	373.2	404.1	434.9
Secondary Sph. Aber. (nm)*	114.2	121.3	128.5	53.6	47.2	40.8
IOL power (D)	20					
RMS (nm)	63.1	55.4	49.4	232.4	281.8	334.9
Sphere (nm)	0.6	0.4	0.3	1.9	1.1	-1.6
Spherical aberration (nm)	-4.8	-3.5	-2.6	218.3	275.6	333.7
Secondary Sph. Aber. (nm)*	63.4	55.9	49.9	90.8	78.2	65.6
IOL power (D)	30					

RMS (nm)	51.5	43.5	37.4	160.0	209.5	280.3
Sphere (nm)	0.2	0.1	0.1	5.9	2.8	-0.2
Spherical aberration (nm)	-2.1	-1.3	-0.8	99.3	183.2	270.5
Secondary Sph. Aber. (nm)*	52.1	44.1	37.9	126.4	108.1	89.8
IOL power (D)	40					
RMS (nm)	52.4	41.4	33.3	170.0	211.5	305.9
Sphere (nm)	0.1	0.1	0.0	8.8	3.9	-1.1
Spherical aberration (nm)	-1.3	-0.6	-0.1	47.7	163.5	288.9
Secondary Sph. Aber. (nm)*	53.2	42.0	33.8	161.2	138.0	115.1

In the results of the second experiment we did not include the RMS and geometrical radii of the spot on the retina because they are more or less the same with the ones from the first experiment. The differences in these results were only for the designs that result in large numbers of Zernike coefficients. These lenses are the lenses with asphericities on the posterior surface. They are not ideal for our models, because their optical quality is really poor when compared with the ones with asphericities on the anterior surface.

(figure available in printed version)

Figure 3.4 *Wavefront RMS error versus IOL power for asphericities designed on anterior and posterior surfaces for IOLs with anterior surface power distribution of 70%, 75% and 80% in respect.*

In figure 3.4 are graphically shown the results of table 3.2. It is obvious that the asphericities of the IOL should be designed in the anterior surface as such a design offers a better optical quality.

Conclusions

In this study the main purpose was to compare optical results of IOLs with a given dioptric power and with different optical designs. In this way of thinking two projects were executed.

Power distribution on spherical lenses

In the first project the optical results of IOLs with a given optical power and with different power distribution between its surfaces were compared. In total five different

dioptric powers were used and these were -0, 10, 20, 30 and D. For each dioptric power 5 different power distributions were implemented. These 0%, 25%, 50%, 75% and 100% of the total dioptric power on the anterior surface and the rest was on the posterior surface. All the lenses in this project were spherical.

From figures 3.2 and 3.3 can be observed that for IOLs with low dioptric powers (e.g. -10, 10 and 20 D) the optical quality is not changing that much with the different power distributions. For greater dioptric powers is obvious that there is a larger difference between the results. It could be advised that the optimal power distribution could be ~75% of the total dioptric power to be given on the anterior surface, while the rest is on the posterior surface. In this way the total RMS error of the eye model (which simulates an average eye that needs an IOL of that power) is the smallest that could be achieved with a spherical monofocal IOL for far vision.

One more thing that could be observed from figure 3.3 is that the total RMS error is actually following the spherical aberration coefficient. This is the main parameter that composes the result of the wavefront error and this should be corrected in the next project with the asphericities on the surfaces of the lenses.

IOL surface asphericities

In the second project, the results of the first were needed. Thus, we used the conclusion from the first project that the 75% of the total dioptric power has to be given on the anterior surface for better optical quality results. In this project, the purpose was to compare a small range of power distributions (between 70% and 80%) in addition to asphericities designed either on the anterior or the posterior surface of the IOL.

From the results in table 3.2 and in figure 3.4 can be observed that better optical quality is provided to the optical system (theoretical eye model) when the asphericities are designed on the anterior surface of the IOL. If they are designed on the posterior surface, then the wavefront RMS increases and the optical quality decrease dramatically. An image simulation in figure 3.5 is showing these results.

(figure available in printed version)

Figure 3.5 *Letter F simulation on the eye model retina. Image size is 96.4 μm for each image and the letter F is a 20/20 size placed in a distance larger than 6 m.*

From figure 3.5 is obvious that when the asphericities are placed on the posterior surface of the lens the optical quality decrease. Here we have to note that if more asphericity orders are added to the design of the lens then the quality of the results increases. More asphericity orders are used in general for multifocal diffractive IOLs where the asphericities have to be designed on the posterior surface when the diffractive pattern of the lens is on the anterior surface.

For the IOL with -10 D of power both designs offer a low optical quality. This could be fixed also with more asphericity orders added in the design.

From the results can also be observed that a power distribution of 75 – 80% has to be given on the anterior surface of the IOL. In this way, a better optical result could be obtained in the end.

Concluding, for IOL designing, it is better to design a 75 – 80% of the optical power on the anterior surface of the lens. When asphericities have to be added, it is better to be added on the anterior surface of the lens as well. If this is not possible (because of diffraction pattern designs etc.) then the asphericities have to be designed on the posterior surface of the IOL and more asphericity orders have to be considered.

Chapter 4.
Visual results simulation with combinations of optimized and non-optimized monofocal correcting elements

Introduction

Cataract surgery is a well-established and a very efficient practice to counteract the optical defects caused by cataract. In such a procedure the cataractous crystalline lens of the human eye is replaced with an IOL. There are many IOL types for a surgeon to choose from, like monofocal or multifocal (which address the loss of accommodation due to presbyopia),[44] having spherical or aspheric surfaces,[48] high-order-aberration-free or correcting IOLs.[50] There has been a lot of research on these IOLs and extensive studies on their optimization. Various cost functions have been considered, ranging from optimizing a single aberration term such as, for example, the spherical aberration to optimizing a certain retinal image quality metric, such as the wavefront mean square error or spatial frequency measures.[51-53]

Although safety and efficacy outcomes of cataract surgery are very high, occurrences of non-optimal implementation of the IOL have also been reported, such as small decentration and tilt of the implanted IOL.[54, 55] IOL power calculation and lens selection are important factors,[47] which might also lead to some errors if not assessed accurately. In such cases a final diffraction error could reach up to ±2 dioptres (D) and result in uncorrected astigmatism, blurred vision, or photic phenomena.[56-58] Overall, such implementations, although not optimal, could still result in a successful surgery, when the quality of life of a post-cataract patient is considered. On the other hand, some patients may need to address this kind of non-optimality either by resorting to a secondary surgery,[59-62] or by using spectacles or CLs.

Another implementation is that the IOLs that are produced and used come in stepped powers of either 0.25 or 0.5 D. This means that there is often a small residual power between the estimated power that an eye needs and the IOL power that is available.

Following cataract surgery, misalignment of IOL and its impact upon the optical performance of an eye have been measured and studied.[63, 64] In those studies, optical performance evaluation is usually conducted using ray-tracing software (e.g., Zemax or OSLO) that simulates a theoretical eye model and calculates the optical results it provides.[50, 52, 64]

In this context, the aim of our study was to calculate and compare the optical and visual outcomes of a range of customized IOL designs, both with and without rounding their

powers to the closest 0.25 D. All calculations have been performed on-axis, in order to study foveal visual quality. Additionally, designs that combine an IOL with a rigid CL were considered, in order to assess situations which are affected by errors that are mentioned above. The tolerance of a particular design to misalignment was also investigated.

Methods

Human eye model

The optical design customization is based on a pupil-cantered version of an anatomically accurate eye model of Liou and Brennan,[17] in which the first surface has been replaced with an estimate of anterior cornea based on real subject measurements. In this sense, retrospective anonymized corneal height data from 22 normal subjects aged 18 to 35, with no corneal surgeries, were used. Noting that the corneal topography does not change much with age, these data facilitated the statistical analysis of the considered designs. Alternatively, statistical eye models could have been used.[65] The topographies had been recorded with an E300 videokeratoscope (Medmont Pty Ltd, Melbourne, Australia). Data collection was approved by the University Ethics Committee and adhered to the tenets of the Declaration of Helsinki. A written consent was obtained from all participants.

Data were divided into two groups according to their corneal-height maps. One group comprised 10 corneas that had no substantial asymmetries (normal group) and the second one (astigmatic group) included 12 astigmatic corneas; that is, having corneal astigmatism above 0.75 D. No other biometric data from those subjects were used in our study.

The raw corneal height data, limited to a central circular 6-mm diameter area, was fitted with the set of fourth-radial-order Zernike polynomials using a least-squares procedure.[66] These estimated Zernike polynomial coefficients were then fed into the ray tracing sofware.

The ray tracing sofware nomenclature[67] used in this paper is indicated by means of Italics font. An incoming ray field of 0 degrees and a wavelength of 587.6 nm are used, which corresponds to the middle default wavelength set for visible spectrum. Monochromatic aberrations for a 3 mm pupil diameter were considered. Unless otherwise

stated, all parameters used in this study are the same as those in the original Liou-Brenan model.[17]

The anterior corneal surface in the model is chosen to be a *Zernike Standard Sag type*. The radius of curvature is set to be infinite and the conic constant is set to 0 in the *Lens Data Editor*. The Zernike coefficients of each cornea are added in the *Extra Data Editor*. Since the estimated corneal height Zernike coefficients are based on discrete data, they do not constitute a truly orthogonal system. That is why the constant equivalent corresponding to

$$c_0^0 - \sqrt{3}c_2^0 + \sqrt{5}c_4^0$$

is not necessarily equal to zero. We can take advantage of this apparent drawback and make use of it to simulate some variability in central corneal thickness (CCT). The group average CCT (mean ± standard deviation), as measured in the ray tracing sofware, was found to be 542 ± 5 µm and 536 ± 12 µm for the normal and the astigmatic group, respectively.

The eye's axial length was optimized in the ray tracing sofware. For this purpose, a *Default Merit Function* is used, which minimizes the wavefront root mean square (RMS) error at the retinal plane. This exact same merit function is used for all optimization procedures mentioned in this paper. Considering the vitreous thickness, it was set as a variable parameter for this optimization, and the group average axial length, as measured in the ray tracing sofware, was found to be 24.32 ± 0.68 mm and 23.89 ± 0.62 mm for the normal and the astigmatic group, respectively.

Hence, we simulated the two resulting sets of eye models with the abovementioned corneal thickness and axial length values, which are all within physiological limits.[17, 68]

The design of correcting elements

The eye models with correcting elements considered in this study include an IOL replacement of the crystalline lens. For some designs, a corrective CL is also added (figure 4.1). In order to simulate an IOL substitution in the models described above, the crystalline lens of the Liou-Brenan model is replaced by a *Non Sequential Component* space of the same thickness and having the same refractive index as the aqueous (1.336).

IOLs are simulated in the ray tracing sofware with the *Toroidal Lens Object Type* in the *Non Sequential Component Editor*. Although a *Toroidal Surface* in *Sequential Mode* would

provide faster optimization, the *Non Sequential Mode* for the simulation of the remaining capsular bag which will host the IOL was chosen in order to facilitate *Macro Order* programming for the IOL misalignments, as it will be described below. Nevertheless, both methods provide the same simulation results and the optimization speed not the particular aim of the study.

The IOLs have all in common the following parameters: diameter of 6 mm, thickness of 1 mm and a constant refractive index of 1.55. They are positioned 1 mm behind the pupil and centered on the optical axis. Their posterior surface is set to have 5 D of optical power (radius of curvature of –42.8 mm) and no asphericity or conic constant.

CLs are simulated in the ray tracing sofware by adding, in the *Lens Data Editor*, four surfaces in front of the anterior corneal surface. The anterior CL surface is simulated as a *Toroidal Surface Type* and it is placed between two *Coordinate Break surfaces*. This is performed to correct the model astigmatism by rotating the surface around the optical axis and selecting different radii of curvature for the sagittal and the tangential axes. The second coordinate break surface has to take the *Pick Up Solve* with a factor of –1 on the *Tilt Around Z* variable. For all CLs, the thickness is set to be 0.1 mm, the diameter is 12 mm and the refractive index is 1.42. The simulated CLs are assumed to be rigid. The posterior surface of the CL is the *Standard Surface Type* with a curvature that follows the cornea without touching it. This curvature is always calculated to have a dioptric power that ranges between –10.5 and –9.5 D (i.e., a radius of curvature between 7.905 mm and 8.737 mm) with a 0.25 D step. The tear film is simulated to have a central thickness of 0.05 mm and a refractive index of 1.337.

For each group of eye models, three additional subgroups were created representing different combinations of IOLs and CLs. These lenses are either optimized to be ideal for each model, resulting in an emmetropic aberration free eye or to resemble real lenses,

(figure available in printed version)

Figure 4.1 *Eye models simulated in the ray tracing software.*

(i) Liou-Brenan model, a. cornea, b. aqueous, c. pupil, d. crystalline lens, e. vitreous, f. retina

(ii) Liou-Brenan model having an IOL instead of the crystalline lens

(iii) Liou-Brenan model having an IOL and a CL.

characterized with discrete spherical and/or toric power.

The optimized ideal lenses are designed using the *Default Merit Function* of the ray tracing sofware. The pupil diameter was always set to be 3 mm and the target distance was far (>6m). This was implemented because in this study monofocal correction at infinity was the main topic. The optimization was done in two steps. The first one was to optimize the radius of curvature of the lens and the astigmatism, in order to create the best focused image on the fovea. The second was to minimize the total wavefront RMS error of the eye model, so that the focused image would be clear.

The real lenses are also optimized but have powers in steps of 0.25 D, which means that the first optimization step was not implemented. The subgroups include:

The models belonging to the optimized IOL group (opt-IOL) include all optimized IOLs, but each IOL has a different anterior surface design, defined by means of the following six variables: sagittal and tangential radius of curvature, conic constant, the second and the fourth order of asphericity and angle of rotation around the optical axis. This last parameter is used to correct the astigmatism of a model.

The models belonging to the real IOL group (real-IOL) include all optimized IOLs (similarly to the opt-IOL group) but in this case the lenses can only have specific power values in steps of 0.25 D. Also, in this group an insertion error of 0.25 D is added, in order to simulate a possible induced refractive error from wrong positioning or power calculation.

The models belonging to the real IOL and CL group (real-IOL+CL) include IOLs from the real-IOL group together with real CLs. Similarly to the real IOLs mentioned above, the real CLs' anterior surface can only have specific power values varying in steps of 0.25 D.

Visual quality metrics

The RMS error of a wavefront, which is used in the optimization procedure for all the designs under evaluation, is not the best metric to evaluate retinal image quality. A popular alternative to the wavefront RMS error is the visual Strehl ratio, which is based on optical transfer function (VSOTF). The VSOTF is considered to be one of the best metrics for assessing retinal image quality,[69] and has been used in many research studies. It is calculated as a ratio of the system's integrated optical transfer function modulated by the contrast sensitivity function to its equivalent for a diffraction-limited system,[70]

$$VSOTF = \frac{\int_{-\infty}^{\infty}\int_{-\infty}^{\infty} CSF_N(f_x, f_y) * OTF(f_x, f_y) df_x df_y}{\int_{-\infty}^{\infty}\int_{-\infty}^{\infty} CSF_N(f_x, f_y) * OTF_{DL}(f_x, f_y) df_x df_y},$$

where $OTF_{DL}(f_x, f_y)$ represents the diffraction-limited optical transfer function, $CSF_N(f_x, f_y)$ is the neural contrast sensitivity function, and (f_x, f_y) are spatial frequency coordinates.

The ray tracing results that the sofware provides, are fed into a custom-written program in Matlab (The MathWorks, Inc., Natick, USA) to yield estimates of the total RMS wavefront error and VSOTF for each model and for each subject's corneal height data. The program uses as input the wavefront function which is produced from the customized anterior cornea and the pupil function that we implement in the ray tracing sofware (circular with 3 mm diameter). By combining these two, it calculates the pupil function which, after Fourier transforming, provides the point-spread function. A secondary Fourier transform yields the optical transfer function (OTF) of the system. The program also calculates the diffraction limited OTF (OTF_{DL}) and the neural contrast sensitivity function (CSF_N) of the system.[71] Finally, it combines the OTF, OTF_{DL} and CSF_N in order to calculate the VSOTF of the system. Figure 4.2 provides a graphical approach of the algorithm.

(figure available in printed version)

Figure 4.2. *A schematic of the custom algorithm written in Matlab.*

Investigating IOL tilt and decentration

To study the effect of IOL tilt and decentration, a *Macro Order* is created introducing either IOL tilt or decentration into all considered models. The program saves the Zernike coefficient text files. Tilts ranged between 0 and 5 degrees of magnitude at steps of 1 degree. Decentration values ranged between 0 and 1 mm at steps of 0.25 mm. Also, the tilt and decentration values are introduced in all directions, at steps of 45 degrees (8 directions in total). The data are processed in the same manner as above and the results (wavefront RMS error and VSOTF) are statistically analysed separately for tilt and decentration values.

Statistical analysis

The statistical analysis includes standard descriptive statistics and hypothesis testing. Since normality of the data, tested with the Jarque-Bera test, was not rejected, standard paired t-test is used to ascertain differences between the various designs. Also, one-way and two-way parametric ANOVA are used. Homogeneity of variance is tested using Levene's test. The level of significance is set to 0.05 for all tests.

Results

Metrics comparison

Table 4.1 shows the group averages (mean ± standard deviation) of the wavefront RMS error (shown in wavelengths of 587.6 nm) and VSOTF while in figure 4.3 those results are graphically depicted.

Table 4.1 *Group average values (mean ± standard deviation) for the wavefront RMS error and VSOTF for all designs under study. The "crystalline lens" row refers to the designs based on the original Liou-Brenan model (with the crystalline lens).*

Metric	Model group	normal	astigmatic
RMS error (wavelengths)	crystalline lens	0.266±0.110	0.922±0.418
	opt_IOL	0.114±0.023	0.122±0.050
	real_IOL	0.176±0.022	0.186±0.045
	real_IOL+CL	0.094±0.029	0.105±0.028
VSOTF	crystalline lens	0.227±0.200	0.014±0.027
	opt_IOL	0.333±0.160	0.362±0.188
	real_IOL	0.326±0.101	0.285±0.107
	real_IOL+CL	0.569±0.121	0.509±0.090

(figure available in printed version)

Figure 4.3 *Group average wavefront RMS error and VSOTF for the normal and the astigmatic eyes groups (RMS measured in wavelengths). The error bars represent one standard deviation. The dashed line indicates a threshold of Cheng et al. corresponding to logMAR=0.* [27]

In both the normal and the astigmatic eyes groups, it is the combination of an IOL and a CL that provides the best optical quality (even better than a perfectly optimized IOL).

For the astigmatic eyes group there is a large difference between the models having the crystalline lenses and the ones corrected with IOLs or with a combination of IOLs and CLs. This may be due to two reasons: the total error induced by the corneal astigmatism and the fact that in our study we only used real anterior corneal height data to feed the different models, while the rest of the model surfaces were rotationally symmetric. This increases the astigmatic effect while, in a real eye, this might be compensated by the internal astigmatism of the crystalline lens. Table 4.2 shows the p-values resulting from the paired t-tests between each pair of designs for the normal eyes group. There are statistically significant differences ($p<0.05$) in VSOTF between the optimized or real IOL models and the combination of IOL and CL.

Table 4.2 *The results of pairwise comparison of the designs for the normal eyes group (paired t-test, p-values)*

	Model groups	opt_IOL	real_IOL	real_IOL+CL
RMS	crystalline lens	<0.001	0.018	0.001
	opt_IOL		<0.001	0.043
	real_IOL			<0.001
VSOTF	crystalline lens	0.038	0.112	<0.001
	opt_IOL		0.449	0.001
	real_IOL			0.001

Table 4.3 shows the p-values resulting from the paired t-tests between each pair of designs for the astigmatic eye group. There are again statistically significant differences ($p<0.05$) in VSOTF between the optimized or real-IOL subgroups and that of the IOL + CL combination.

Table 4.3 *The results of pairwise comparison of the designs for the astigmatic eyes group (paired t-test, p-values)*

	Model groups	opt_IOL	real_IOL	real_IOL+CL
RMS	crystalline lens	<0.001	<0.001	<0.001
	opt_IOL		<0.001	0.127
	real_IOL			<0.001
VSOTF	crystalline lens	<0.001	<0.001	<0.001
	opt_IOL		0.053	0.014
	real_IOL			<0.001

Decentration and tilt of the IOL

Figure 4.4 depicts, for both groups, how the average VSOTF (across all eight directions and all subjects) changes as a result of IOL decentration. For the normal-eyes group (figure 4.4a), the VSOTF for the real_IOL+CL subgroup shows a greater drop compared to the other two subgroups (opt_IOL, real_IOL) as the decentration increases. On the other hand, for each particular level of decentration, it is the real_IOL+CL subgroup that provides the best average VSOTF. Furthermore, for each decentration level, the real_IOL+CL subgroup average VSOTF is better than that obtained for the opt_IOL subgroup in the previous (smaller) decentration step. In addition to this, we observe that for a 0.5 mm decentration

the real_IOL+CL subgroup average VSOTF is higher than that of the centred opt_IOL and at 0.75 mm it is approximately the same. The opt_IOL and real_IOL subgroup average VSOTF decreases in the same manner. Statistically significant differences (one-way ANOVA, $p<0.05$) in average VSOTF are found for decentration values up to 0.5 mm. Two-way ANOVA revealed statistically significant changes in average VSOTF between the models and the magnitude of decentration (both p-values less than 0.001) but not for the interactions ($p=0.073$).

Similar observations can be made for the astigmatic eyes group (figure 4.4b). Similarly to the normal-eye group, the graph reveals that the average VSOTF for the real_IOL+CL subgroup shows a greater drop with decentration compared to the other two subgroups. However, for each particular decentration level it is precisely the real_IOL+CL subgroup the one that provides the best optical quality outcomes (i.e., the highest average VSOTF). For up to 0.75 mm of decentration, the average VSOTF for this real_IOL+CL subgroup exceeds that of the opt_IOL subgroup at the previous (lower) decentration step. Similarly to the normal eyes group, statistically significant differences (one-way ANOVA, $p<0.05$) in average VSOTF were found for decentration values of up to 0.5 mm in the astigmatic group. Again, two-way ANOVA revealed statistically significant changes in average VSOTF between the models and the magnitude of decentration (both p-values less < 0.001) but not for the interactions ($p=0.276$).

(figure available in printed version)

Figure 4.4 *Average VSOTF vs. IOL decentration in all directions (a) for the normal eyes group and (b) for the astigmatic eyes group. The dashed line indicates a threshold of Cheng et al. corresponding to logMAR=0.* [27]

Figure 4.5 shows the average VSOTF (across all eight directions and all subjects) as a function of IOL tilt angle. In the normal eyes group (figure 4.5a) we observe that it is the opt_IOL subgroup that is affected the least by tilt (i.e., that the average VSOTF decreases the least with tilt). The real_IOL subgroup, for small tilts angles (1 to 2 degrees), follows the opt_IOL subgroup's trends, while for larger tilts it shows a faster drop. As for the real_IOL+CL subgroup, it consistently provides a better optical quality than all the other subgroups: even in the worst-case scenario (5-degree tilt) it outperforms the other two subgroups in the no-tilt situation. On the other hand, it is worth pointing out that it shows the largest VSOTF drop (in absolute terms) between 0 and 5 degrees. Statistically significant differences (one-way ANOVA, $p<0.05$) in the average VSOTF were found for all angles of tilt. Two-way ANOVA revealed statistically significant changes in the average VSOTF between the models ($p<0.001$) and the magnitude of tilt ($p=0.001$) but not for the interactions ($p=0.930$).

The same observations can be made for the astigmatic eyes group (figure 4.5b). There is a similar decreasing trend for the opt_IOL and real_IOL+CL subgroups, while the real_IOL+CL one provides the highest average VSOTF values for any given tilt angle. Statistically significant differences (one-way ANOVA, $p<0.05$) in the average VSOTF were found for all angles of tilt. Again, two-way ANOVA revealed statistically significant changes in the average VSOTF between the models ($p<0.001$) and the magnitude of tilt ($p=0.001$) but not for the interactions ($p=0.999$).

Decentration in different directions

3.1 Astigmatic eyes group

(figure available in printed version)

Figure 4.5 *Average VSOTF vs. IOL tilt in all directions for the (a) normal eyes and (b) astigmatic eyes group. The dashed line indicates a threshold of Cheng et al. corresponding to logMAR=0.* [27]

Further, we analysed the impact of IOL decentration upon optical quality (average VSOTF) in specific directions, and the results are shown in figure 4.6. Almost no decrease is observed if the IOL is decentred along the flat astigmatic axis (figure 4.6a), while IOL decentration along any other direction (excluding the flat astigmatic axis) leads to a larger drop (figure 4.6b). Again, for any given decentration scenario it is the real_IOL+CL subgroup that reached the highest average VSOTF values.

For decentration values along the flat astigmatic axis, statistically significant differences (one-way ANOVA, $p<0.05$) in average VSOTF were found for all decentration values. Two-way ANOVA revealed statistically significant changes in the group average VSOTF only between the models ($p<0.001$). For decentration values along all the other directions (i.e., excluding the flat astigmatic axis), statistically significant difference (one-way ANOVA, $p<0.05$) in average VSOTF was only found for the zero-decentration scenario. Two-way ANOVA revealed statistically significant changes in the group average VSOTF between the models and the magnitude of decentration (both p-values less than 0.001) and for the interactions ($p=0.017$).

Figure 4.6 *Astigmatic eyes group average VSOTF vs. IOL decentration (a) along the flat astigmatic axis and (b) in all other directions. The dashed line indicates a threshold of Cheng et al. corresponding to logMAR=0.* [27]

(figure available in printed version)

3.2 Normal eyes group

If we consider the normal-eyes group as a group of eyes showing a certain degree of astigmatism, then we will observe the same trend for the flat astigmatic axis and all the other directions of decentration, as illustrated in figure 4.7a and 4.7b.

For decentration values along the flat astigmatic axis, statistically significant differences (one-way ANOVA, $p<0.05$) in average VSOTF were found for all decentration values. Two-way ANOVA only revealed statistically significant changes in average VSOTF between the models ($p< 0.001$). For decentration values along all other directions (i.e., excluding the flat astigmatic axis) statistically significant differences (one-way ANOVA, $p<0.05$) in average VSOTF were found for up to 0.25 mm of decentration. Two-way ANOVA revealed statistically significant changes in average VSOTF between the models and the magnitude of decentration (both p-values < 0.001) and for the interactions ($p=0.030$).

(figure available in printed version)

Figure 4.7 *Normal eyes group average VSOTF vs. IOL decentration (a) along the flat astigmatic axis and (b) in all other directions. The dashed line indicates a threshold of Cheng et al. corresponding to logMAR=0.* [27]

Discussion

Assessing the optical and visual quality of ocular correcting elements using simulations and eye modelling constitutes a major part of the IOL design [1]-[8], [26] as well as that of CL [27]. Our study further contributes to the field of simulating visual quality results by using combinations of ocular correcting elements. We calculated and compared the simulated optical and visual quality results yielded by customized eye models that included IOLs and CLs. Our aim was to determine whether either an optimized or a corresponding robust design is appropriate to be implanted and whether or not the combination of an IOL and a CL provides better results in the presence of a residual refractive error. Furthermore, we simulated different degrees of misalignment (decentration and tilt values) and assessed the resulting tolerance of each design. Customization of each design was possible through the addition of real anterior corneal topography data. This, in turn, allowed performing statistical analysis of the results and seeking whether differences between the designs are statistically significant.

For both the normal and astigmatic eyes groups we found that the implantation of a robust IOL instead of a fully optimized one leads to poorer visual results. Nonetheless, this quality drop is neither statistically nor clinically significant compared to the limit proposed by Cheng et al. (which corresponds to 0 logMAR visual acuity),[72] as shown in figure 3. Also, we observed that visual performance increases when a CL is applied to the model that includes an IOL. In this case the increase is large and statistically significant. Also, although the increase in optical quality above the Cheng's limit may seem to be unwarranted, it provides larger tolerance boundaries in case of misalignments.

While simulating IOL decentration we observed that the VSOTF for the IOL+CL subgroup shows a faster drop, but it always exceeds that of the other two designs (see figure 4). A similar trend was observed for lens tilt (figure 5). Furthermore, with a tilted IOL the VSOTF for the IOL+CL subgroup is better than that of the other designs even with no tilt. The visual acuity in these simulations gets below the 0 logMAR when large misalignments take place (larger than 0.5 mm decentration and 3 degrees of tilt). It is obvious though that

the combination of two correcting elements (IOL and CL) provides better tolerance in large misalignments by keeping the visual quality above the Cheng's limit.

When simulating IOL decentration, we observed that VSOTF drops faster along any direction different from the flat astigmatic axis (figures 6 and 7). This happens also in the normal eyes group, characterized with a small amount of astigmatism. The direction of the decentration plays a significant diminishing role (at least for higher amounts of decentration) in the optical quality of the system. Furthermore, there is slight decrease below the Cheng's limit when the decentration is on the flat axis and a large decrease when the decentration is towards all other directions. That trend is more pronounced for the real_IOL+CL design, similarly to what was revealed for the group of astigmatic subjects. On the other hand, the diminishing trend of opt_IOL has achieved levels of significance for higher amounts of IOL decentration than the other two designs. This could suggest that in a real-life scenario more attention should be given to the decentration direction of the IOL implant. We also noted that the combined IOL+CL model is the one providing the best visual outcomes.

Finally, throughout our work we found that this enhanced VSOTF that the IOL+CL design provides is useful, since it extends the tolerance boundaries for misalignments. As the misalignment increases VSOTF decreases, but for small misalignments up to 0.5 mm of decentration and up to 5 degrees of tilt the difference is statistically significant and clinically relevant.

Chapter 5.
Visual results with combinations of optimized and non-optimized bifocal correcting elements

Introduction

Presbyopia and cataract are two common pathologies that appear in the age of 50 years and derange the visual quality. The effects of these pathologies advance as people get even older and as a result, people of this age that are still energetic and productive, face vision issues that keep them away from their jobs and make their life more difficult.

Presbyopia affects all people and its symptoms appear between the ages of 45 and 55 years. The main symptom is that the patient is no longer able to accommodate on near targets such as a book or a computer screen and he needs visual aid to do short distance work. The main reason is that the crystalline lens of the eye becomes thick and stiff, unable to accommodate and focus correctly the image on the retina.[4, 7, 42]

In addition, this people with cataract have a blurry image with low contrast as a final result. This is because the crystalline lens gets foggy and thick, dispersing the light instead of focusing. Cataract usually appears after 55 years old, although some people are diagnosed earlier with cataract.[43]

In order to solve these refractive issues of the crystalline lens, a common practice is to replace it with an IOL. These IOLs are used widely and there is a lot of research going on around them and the results that they offer.[14, 47, 59]

There are a lot of different IOLs in the market. IOLs with different materials, dioptric powers and ultraviolet filters. Monofocal or multifocal, with two or three foci.[44, 48] There are multifocal lenses which provide multifocality either with refractive zones of different dioptric power or with diffractive patterns. The last ones use the diffraction pattern in order to divide the incoming light and focus it in two or three focal points in the same time.[45] There are also some accommodative IOLs that claim to accommodate depending on the target distance by using the ciliary muscle that is used to accommodate with the crystalline lens.

The study of diffractive multifocal IOLs is the main purpose of this study. Specifically, the design of diffractive multifocal IOLs and simulation of their optical and visual results in theoretical human eye models that are customized. The customization of these models concerns the anterior cornea of the eye model in this study. There have been carried on other studies too that use customized eye models for IOL simulations.[52, 54]

In our knowledge, there is no such study that simulates results of optical and visual quality with diffractive multifocal IOLs. As an additional step, in this study are used topographic data from corneas of patients in order to have a population of different eye models. For these eye models, two types of diffractive IOLs were designed. The first one was an optimized IOL that was exactly designed for this eye model. The second one, was not optimized, but followed the rule of the IOLs in the market with distinct power in steps of 0.25 D. A comparison was made between these IOLs and their results in order to see if the optimization of an IOL is truly worthy to be implemented.

As a continuation of this study, some decentrations and tilts were introduced in the system affecting the position of the IOL in the eye model. A second comparison between the final results of the misaligned system will provide knowledge about the tolerance of the designed IOLs in misalignments.

Methods

For the optical design and the simulations in this project, an optical design program was implemented.[49] As a part of the methods in this study, some instructions that include the ray tracing sofware objects will be described. All the ray tracing sofware objects and nomenclature from this point in the manuscript will be noted with Italics in the text. For all the simulations, an incoming ray field of 0 degrees and a wavelength of 587.6 nm were used, which corresponds to the middle default wavelength set for visible spectrum in the ray tracing sofware. Monochromatic aberrations for a 3 mm pupil diameter were considered.

Human eye model

In order to simulate the optical and visual quality of the diffractive multifocal IOLs, a theoretical human eye model was needed. The Liou-Brennan eye model[17] was used in this study. Although there are many models,[15, 19, 25, 73, 74] older and new ones with a lot of details to be used, we chose that one because of its simplicity that was enough for our study. In any case, most of the differences between the models regard the crystalline lens of

the eye. In this study the eye models that are used are designed with an IOL instead of a crystalline lens.

The eye models that we used had all the parameters of the original Liou-Brennan model, except from the ones that are clearly noted in this manuscript. The pupil of the model was set always at 3 mm diameter. This diameter is usually found in elderly people or in light conditions, which are the conditions that we were interested in.

The anterior corneal surface of the model was customized. The customization was about the anterior corneal topography. Topographical corneal height data were retrospectively used by 22 normal subjects, aged 18 to 35, with no corneal surgeries. The topographies had been recorded with an E300 videokeratoscope (Medmont Pty Ltd, Melbourne, Australia). Data collection was approved by the University Ethics Committee and adhered to the tenets of the Declaration of Helsinki. A written consent was obtained from all participants. Although the simulations have as target a different age group, the corneal map is not affected by ageing and it can be used as a mean of randomization for this group.

These data were divided into two groups. One group of 10 corneas that had no asymmetric differences (normal group) and a second one of 12 corneas with astigmatic asymmetries (astigmatic group). The astigmatic asymmetries refer to corneal astigmatism over 0.75 D.

The raw corneal height data from the topographer were limited in a 6 mm diameter area. They were fitted with a set of fourth-radial-order Zernike polynomials using a least square procedure.[66] This procedure was done with Matlab R2012b. The fitted data, resulted in Zernike coefficients which were then fed into the ray tracing sofware.

In the optical design program, the anterior corneal surface was set as a Zernike Standard Sag type. The radius of curvature was set to be infinite and the conic constant was set 0 in the Lens Data Editor. All the information needed for the anterior cornea were given by the Zernike coefficients, which were introduced in the Extra Data Editor. Since the estimated corneal height Zernike coefficients are based on discrete data, they do not constitute a truly orthogonal system. That is why the constant equivalent corresponding to

$$c_0^0 - \sqrt{3}c_2^0 + \sqrt{5}c_4^0$$

is not necessarily equal to zero. We can take advantage of this apparent drawback and make use of it to simulate some variability in central corneal thickness (CCT). The group average CCT (mean ± standard deviation), as measured in the ray tracing sofware, was found to be 542 ± 5 μm and 536 ± 12 μm for the normal and the astigmatic group, respectively.

The model eye total axial length was optimized in the ray tracing sofware. This was done by using the Default Merit Function of the program, which minimizes the wavefront RMS error at the retina, by changing the variables set by the programmer. The same merit function is used in all optimization processes that are mentioned in this manuscript. The vitreous thickness was set as a variable in this optimization process. The group average axial length, measured in the ray tracing sofware, was 24.32 ± 0.68 mm and 23.89 ± 0.62 mm for the normal and the astigmatic group, respectively.

In the end, we simulated the two resulting groups of eye models with the abovementioned corneal thickness and axial length values, which were all within physiological limits.[17, 68]

The design of the optimized IOLs

After designing the eye models and optimizing them, the diffractive multifocal IOLs had to be designed. All the IOLs designed had the following common characteristics. Their central thickness was set to 1 mm, their optical diameter was 6 mm and their position was 1 mm behind the pupil. The refractive index of their material was set at 1.55.

In order to be placed in the eye models, the crystalline lens of the model was removed. In the empty space was designed a Non-Sequential Component space which was given the same refractive index of the aqueous humour that fills the anterior and posterior chamber. This space had a total thickness of 4.02 mm, the thickness of the removed crystalline lens. In this Non-Sequential Component space the IOL was designed as it is shown in figure 5.1.

(figure available in printed version)

Figure 5.1 *Human eye model (i) with crystalline lens and (ii) with IOL in the Non-Sequential Component space. a. Anterior corneal surface, b. Posterior corneal surface, c. pupil, d. crystalline lens, e. vitreous, f. retina.*

Each IOL surface in this project was calculated and designed by using the asphere surface sag formula:

$$z = \frac{cr^2}{1 + \sqrt{1 - (1 + k)c^2 r^2}} + a_1 r^2 + a_2 r^4$$

where z is each surface point height, $c = \frac{1}{R}$ is the curvature of the surface and R is the radius of curvature, k is the conic constant of the surface, r is the radial coordinate of each point, a_1 is the 2nd order and a_2 the 4th order aspheric constant.

Firstly, a monofocal IOL with a single focus at infinity was designed. This was done in order to optimize this IOL and get all the necessary data (radii of curvature and asphericities) for the diffractive IOL. The anterior surface was aspheric and rotationally symmetric, while the posterior was spherical and toric, in order to correct every astigmatic parameter. The optimization was done in three steps. The first one optimized the radius of curvature and the second one optimized the 2nd and 4th order asphericities and the conic constant of the anterior surface of the IOL. Finally, the third step optimized both the posterior surface radii (normal and astigmatic) of curvature and the astigmatic angle. In the end all the geometrical characteristics of the IOL were collected.

All the IOLs designed and used in the project were diffractive bifocal. This was done by dividing the previously designed monofocal IOL into two lenses in the ray tracing sofware that were in touch with each other. These lenses were introduced in the Non-Sequential Component Editor in the ray tracing sofware, in which we used two lines. The first one was for the anterior part of the IOL that carried the diffractive pattern and the second one which was for the posterior part of the IOL which was toric. Both these IOL parts had the optimized data from the previously described optimization method.

The anterior part of the IOL was a Tabulated Fresnel Radial object. This object takes as an input a text file with coordination data in order to design the IOL. The text file was calculated by a custom Matlab code that takes as input the geometrical data of the IOL and of the diffractive pattern that is going to be designed. For the diffractive pattern the data

were for the step height to be half of the wavelength, with ten diffractive zones, central refractive diameter of 1 mm and near dioptric power of 3.25 D. The Matlab code created the coordinations for the design and these coordinations were fed in the ray tracing sofware that designed the final diffractive anterior lens.

The posterior part of the IOL was a Toroidal Lens type with the geometrical data from the optimized monofocal IOL. These would be the normal and the astigmatic radii of curvature and the angle of astigmatism.

The design of the robust IOLs

In order to simulate also some more realistic IOLs the previous design was altered. Each IOL surface power was changed to the closest 0.25 D stepped power. This change was implemented by changing the radius of curvature of each surface. In this way, the IOLs were changed and simulated more realistic IOLs that carry dioptric power in the same steps. The diffractive patterns and the rest designing methods were the same as previously described.

Optical and visual quality metrics

The wavefront RMS error is a common quality metric to evaluate the optical quality of an optical system. This was collected from the ray tracing sofware after performing a Ray Tracing procedure. In order to calculate the visual quality evaluation, which is the main topic of this project, an alternative metric was used called visual Strehl ratio. The VSOTF is considered to be one of the best metrics for assessing retinal image quality,[69] and has been used in many research studies. It is calculated as a ratio of the system's integrated optical transfer function modulated by the contrast sensitivity function to its equivalent for a diffraction-limited system,[70]

$$VSOTF = \frac{\int_{-\infty}^{\infty}\int_{-\infty}^{\infty} CSF_N(f_x, f_y) * OTF(f_x, f_y) df_x df_y}{\int_{-\infty}^{\infty}\int_{-\infty}^{\infty} CSF_N(f_x, f_y) * OTF_{DL}(f_x, f_y) df_x df_y}$$

where $OTF_{DL}(f_x, f_y)$ represents the diffraction-limited optical transfer function, $CSF_N(f_x, f_y)$ is the neural contrast sensitivity function, and (f_x, f_y) are spatial frequency coordinates.

The ray tracing results that the software provides, are fed into a custom-written program in Matlab to yield estimates of the total RMS wavefront error and VSOTF for each

model and for each subject's corneal height data. The program uses as input the wavefront function which is produced from the customized anterior cornea and the pupil function that we implement in the software (circular with 3 mm diameter). By combining these two, it calculates the pupil function which, after Fourier transforming, provides the point-spread function. A secondary Fourier transform yields the optical transfer function (OTF) of the system. The program also calculates the diffraction limited OTF (OTFDL) and the neural contrast sensitivity function (CSFN) of the system.[71] Finally, it combines the OTF, OTFDL and CSFN in order to calculate the VSOTF of the system. Figure 5.2 provides a graphical approach of the algorithm.

(figure available in printed version)

Figure 5.2 *A schematic of the custom algorithm written in Matlab.*

IOL misalignments

To study the effects of misalignments (decentrations and tilts) of the IOLs in the eye models, a Macro order was created in the ray tracing sofware. This custom made program was used in order to introduce all the decentrations and tilts, step by step to each eye model, perform the Ray Tracing and save the results for further analysis. Tilts ranged between 0 and 5 degrees of magnitude at steps of 1 degree. Decentration values ranged between 0 and 1 mm at steps of 0.25 mm. Also, the tilt and decentration values are introduced in all directions, at steps of 45 degrees (8 directions in total). This differentiation in directions was needed because the models are not rotationally symmetric and the results are different in general.

Statistical analysis

The statistical analysis includes standard descriptive statistics and hypothesis testing. Since normality of the data, tested with the Jarque-Bera test, was not rejected, standard paired t-test was used to ascertain differences between the optimized and robust designs. Also, two-way parametric ANOVA test was used. Homogeneity of variance was tested using Levene's test. The level of significance was set to 0.05 for all tests.

Results

From the previously described methods, we collected the wavefront RMS error and the Zernike coefficients of each one eye model from the 22 in total, with each optimized and non-optimized IOL in all misalignments as well as in the central position in txt files. These data were fed in the custom made Matlab code, which calculated the VSOTF results (as it is described in Methods section).

For the normal eyes group, paired t-test did not show statistically significant difference between the optimized and the robust design for far target distance (p=0.06) or for near target distance (p=0.11). For the astigmatic eyes group, statistically significant

difference was found for the near target distance (p=0.01) but not for far target distance (p=0.14).

The mean values and the standard deviations of each group are graphically depicted in the following figures.

In figure 5.3 is shown the VSOTF over the decentration for the normal eyes group for far and near target distances. There is also the result for the centered position of the IOL (0 mm decentration in the figure). These are the mean values of the decentrations in all directions.

A two-way ANOVA test revealed for the optimized IOL and for the far target that there were statistically significant changes between the magnitudes of the decentration (p-value < 0.001). No statistically significant differences were found between the directions of the decentration (p=0.1) and for the interactions (p=1). For the robust design at far target distance there were found statistically significant differences between the magnitudes of decentration (p<0.001) and between the direction of decentration (p=0.02) but not between the interactions (p=0.93). For near target distance and for both designs (optimized and robust) there were found statistically significant differences between magnitudes, directions of decentration and for the interactions (all p-values < 0.001).

(figure available in printed version)

Figure 5.3 *Visual Strehl ratio for normal eyes group over decentration for far and near target distances.*

In figure 5.4 is depicted the VSOTF over the decentration for the astigmatic eyes group for far and near target distances. There is also the result for the centered position of the IOL (0 mm decentration in the figure). These are the mean values of the decentrations in all directions.

A two-way ANOVA test revealed for the optimized IOL and for the far target that there were statistically significant changes between the magnitudes of the decentration (p-value < 0.001) and between the directions of the decentration (p=0.03). No statistically significant differences were found for the interactions (p=0.56). For the robust design at far target distance the results of the two-way ANOVA were in the same direction although for this design there were also found statistically significant differences between the interactions of decentration and direction (p<0.001 for the decentrations, p=0.02 for the directions of the decentration and p=0.47 for the interactions). For near target distance and for both designs (optimized and robust) there were found statistically significant differences between magnitudes, directions of decentration and for the interactions (all p-values < 0.001).

(figure available in printed version)

Figure 5.4 *Visual Strehl ratio for astigmatic eyes group over decentration for far and near target distances.*

In figure 5.5 is shown the VSOTF over the tilt for the normal eyes group for far and near target distances. There is also the result for the no tilted position of the IOL (0 degrees of tilt in the figure). These are the mean values of the tilts in all directions.

A two-way ANOVA test revealed for the optimized IOL and for the far target that there were statistically significant changes between the magnitudes of tilt and between the directions of tilt (p-values<0.001). No statistically significant difference was found for the interactions between the magnitude and the direction of tilt (p=0.89). For the robust design at far target distance the same image came out from the two-way ANOVA test (p-values<0.001 for magnitude of tilts and directions of tilt, p=0.53 for the interactions). For

near target distance for the optimized IOL, statistically significant differences were found for the magnitude of tilts (p=0.008) but not for the directions of tilt (p=0.27) or for the interactions between them (p=0.35). For the near target distance of the robust IOL the results of the two-way ANOVA are in the same direction but there is difference in the significance (p=0.01 for the magnitude of tilt, p=0.09 for the directions of tilt and p=0.1 for the interactions between them).

(figure available in printed version)

Figure 5.5 *Visual Strehl ratio for normal eyes group over tilt for far and near target distances.*

In figure 5.6 is depicted the VSOTF over the tilt for the astigmatic eyes group for far and near target distances. There is also the result for the no tilted position of the IOL (0 degrees of tilt in the figure). These are the mean values of the tilts in all directions.

A two-way ANOVA test revealed for the optimized IOL and for the far target that there were statistically significant changes between the magnitudes of tilt and between the directions of tilt (p-values < 0.001). No statistically significant difference was found for the interactions between the magnitude and the direction of tilt (p=0.85). For the robust design at far target distance the same image came out from the two-way ANOVA test (p-values<0.001 for magnitude of tilts and directions of tilt, p=0.71 for the interactions). For near target distance for the optimized IOL, statistically significant differences were found for the magnitude of tilts (p<0.001) and for the directions of tilt (p=0.04) but not for the interactions between them (p=0.92). For the near target distance of the robust IOL the two-way ANOVA showed statistically significant difference between the magnitudes of tilt (p<0.001) but not between the directions of tilt (p=0.15) or for the interactions between the magnitudes and the directions of tilt (p=0.87).

(figure available in printed version)

Figure 5.6 *Visual Strehl ratio for astigmatic eyes group over tilt for far and near target distances.*

Conclusions

In this study diffractive bifocal IOLs, of optimized and robust design, were designed and tested under centered and misaligned positions. The IOLs were designed with a custom made code in Matlab and the designs were introduced in the ray tracing sofware in 22 customized (personalized) eye models. The eye models were designed following the theoretical eye model of Liou-Brennan. The customization was done by changing the anterior corneal surface of the model with retrospective topographical data from 22 real patients.

The results produced after the ray tracing in the optical design program, were in terms of wavefront RMS error and Zernike coefficients, which actually evaluated the optical quality of each system (eye model with IOL). The main interest in this project was in the visual quality evaluation of the models, so the results were fed in a custom made code in Matlab which calculated the VSOTF of each system. The results then, were grouped and statistically analyzed.

From the t-tests which compared the optimized and robust IOLs, was found that there was statistically significant difference only between the designs for the near target distance in astigmatic eyes. For all the other distances and designs, there was no statistical significance between the results. This means that the optimization of the IOLs does not offer any significant difference in the visual quality. Even, for the astigmatic eyes that there was found a statistically significant difference for the near target distance, it is not a clinically significant difference because the difference is not observable from a patient. It is also obvious from the all figures (5.3, 5.4, 5.5 and 5.6) that all the mean values of the VSOTF are changing in the same way (optimized and robust), a fact that supports the conclusion that optimization is not necessary to be done for less than 0.25 D steps.

For decentrations on the far target distance there was found statistically significant difference between the magnitudes of the decentrations. This means that decentration of a diffractive IOL affects strongly the visual quality of a patient. Especially for astigmatic patients that is also important the direction of decentration, because of the astigmatic axis

(statistically significant difference between the directions of decentration). For both normal and astigmatic patients, a decentration of more than 0.25 mm affects strongly the visual quality of the patient and has to be corrected. For near target distances, decentration affects even more the visual quality either by magnitude or by direction. It can be observed that the VSOTF for near target distances increases with decentration. This might be correct as a calculation, but the VSOTF result is so small that the quality increase is not observable. It is only a calculation result, which is small because the near target image that is projected in the retina is somehow blurry, as a result of the diffraction from the diffractive pattern. This calculation result can be altered in the simulations if the pupil diameter is decreased as the target distance decrease.

Regarding the tilts, the magnitude and the direction of tilt affect strongly both normal and astigmatic eyes for far target distances. A tilt magnitude over 3 degrees is not accepted and has to be corrected. For near target distances, the conclusions are almost the same, suggesting that magnitude of tilt is important and affects strongly the final visual quality. There is again the same result, for the near target visual quality and the tilt. It seems that the visual quality increase as the tilt increase, but the increase is small and not observed from the patient (it is not clinically significant).

Concluding, diffractive bifocal IOLs provide two distances of focus for people that can't focus because of presbyopia and cataract. Optimization in steps of 0.25 D of optical power is enough for these IOLs. Visual quality provided for far target distances is good but strongly affected by decentrations and tilts. The near target visual quality provided is not very good, because of the diffraction of light that makes it blurry, but if the pupil decreases its diameter the results will get better. Something that is realistic, because when close distance work takes place (such as reading) more light is needed, which makes the pupil smaller. The misalignments seem to favour near target visual quality, something that is not correct and not clinically significant, as the results are really small and the quality provided poor.

Chapter 6.
Intraocular telescopic system design: optical and visual simulation in a human eye model

Introduction

Loss of vision is an outcome of different pathologies or accidents. Age related macular degeneration (AMD) is a severe pathology that causes loss of central vision. A part of the middle and old aged population of the developed world are diagnosed with AMD. Patients diagnosed with AMD face serious symptoms in their vision, which in the end result in loss of central field of view. This is because AMD affects the central part of the retina (macula) by destroying the photoreceptors. In this situation, patients need to use the peripheral field of view in order to track moving objects and to move in their environment.[75-77] Another age related pathology that is very common for middle aged and older patients is cataract, which results in the blurring of the crystalline lens. This situation is usually faced with cataract extraction surgery and IOL implantation, in order to correct the hyperopia that is caused from the extraction of the crystalline lens.[43]

For patients that are diagnosed with both pathologies, in order to encounter both of them in one surgical procedure, there is a solution of implanting an intraocular telescopic system (ITS). This is a miniaturized telescopic device that can be implanted in the human eye. There have been many trials and research studies about these systems showing the clinical results, safety issues and how these devices improve the life quality of these patients.[78-81] There are two different types of ITS. The first one is composed by 2 lenses with high optical power (Galilean telescope)[82] and the second one is composed by mirrors (Cassegrain telescope).[83] Both ITS project a magnified image, with a magnification of x2 or x3. The Galilean type ITS has been studied and tested in many studies before. There are two different types of Galilean type ITS. One that is positioned between the anterior and posterior chamber of the eye and a second that is positioned totally in the posterior chamber, behind the pupil. These telescopes have been studied before about their optimal position, distance between their lenses and magnification provided.[78, 82, 84]

Then, the purpose of this study is to design both types of Galilean telescopes and simulate optical and visual results in a human eye model. The simulations were made in order to find out which one of the two telescopes should be better for far and near target distances.

Methods

To design and study the optical and visual quality of the ITS, an optical design program was implemented [49, 67]. The human eye model used was the one that Liou and Brennan introduced in 1997[17]. This was selected because it is simple enough for the needs of this study. More complicated and recent models could also be used[19, 22, 50, 74, 85], but the results produced would follow the same pattern if the model simulates an emmetropic human eye. In any case, the main difference between the theoretical eye models is the way that the crystalline lens is designed. In this study, as it will be further explained, the crystalline lens was removed, so there is no major difference if another model is used. Unless otherwise stated in the paper, all the parameters of the model used, were the same as they were presented in the work of Liou and Brennan.

For the simulations, a central incoming field of rays was used, passing through a pupil of 3 mm diameter, with a wavelength of 587.6 nm (green light). The study was based on monochromatic simulations. Two different target distances were used in this study's simulations: a far target distance (far) which is supposed to be larger than 6 m and a near target distance and 0.41 mm (near) which is a close reading distance. As the target distance decreased, the distance between the lenses had to increase in order for the image to be focused correctly.

The ITS that were studied consist of an anterior positive and a posterior negative lens (Galilean telescope). Both lenses were of high optical power as it will be described. Two different ITS were designed and compared. The first one has the positive lens in front of the pupil and the negative lens behind. The second one is totally positioned behind the pupil. All lenses in this study do not represent any real design, material or patent used. They were created for the needs of this specific study, although a future study could introduce a specific design that it is used in common practice.

(figure available in printed version)

Figure 6.1 *Liou-Brennan eye model with intraocular telescope ITS 1. a. cornea, b. anterior positive lens, c. pupil, d. posterior negative lens, e. retina.*

The ITS through pupil (ITS 1) was designed following the work of Felipe et al[82] and the model is shown in figure 6.1. The crystalline lens was removed from the eye model and the empty space was given the refractive index of the aqueous (1.336). The system is composed by a positive anterior lens of 53 D and a negative posterior lens of -64 D. The anterior lens was designed 1.66 mm from the posterior corneal surface and 0.5 mm in front of the pupil. It was a positive lens of 53 D optical power, with a refractive index of 1.55 and thickness of 1 mm. The anterior surface of the lens was given 33 D of power while the posterior surface was calculated to be 20.44 D, in order for the total power to be 53 D in total. This power was calculated from the effective power formula

$$D = P_a + P_p - \frac{t}{n} P_a P_p.$$

In this formula D represents the total optical power in Diopters, P_a, P_p the optical powers of the anterior and posterior surface of the lens respectively, t the thickness and n the refractive index of the lens. The posterior lens was designed behind the pupil, in a distance of 2.6 mm from it. It was a negative lens of total power -64 D. The anterior surface was given the power of -34 D and the posterior surface was calculated to be at -29.36 D. The same thickness and refractive index was used in the power calculation formula as mentioned before. The total distance between the lenses therefore was 3.1 mm for the far target distance and 3.65 mm for the near target distance. The ITS behind the pupil (ITS 2) design was based on the work description of Tabernero et al[84] and the model is shown in figure 6.2.

(figure available in printed version)

Figure 6.2 *Liou-Brennan eye model with intraocular telescope ITS 2. a. cornea, b. pupil, c. anterior positive lens, d. posterior positive lens, e. retina.*

As previously mentioned, the crystalline lens was removed from the eye model. The empty space was given the refractive index of the aqueous and the whole telescopic system was designed behind the pupil, in the posterior segment. This system is composed by a

positive anterior lens of 66 D and a negative posterior lens of -66 D. For the positive lens, the anterior surface was designed with 36 D of optical power and the posterior surface was calculated to have power 30.71 D. For the negative lens, the anterior surface was designed with -36 D of power and the posterior was calculated to have -29.32 D of power. All calculations were done as mentioned before, with the calculation formula of thick lens power. Both lenses had thickness of 1 mm and refractive index of 1.55. The distance between the lenses in this system was 1.5 mm for the far target distance and 1.95 mm for the near target distance.

Optimization and decentration of the lenses

Both ITS were studied under optimized and non-optimized situations. The optimization process was done through the ray tracing sofware with the optimization tool that the program provides. This tool optimizes the system by changing the variables that the user selects in order to get the least RMS wavefront error of the whole optical system. The variables that were used in this study were the conic constant, the second and fourth asphericity term of the anterior surface of the positive lens of the system. These were selected in order to study the differences between an ITS with spherical lenses and an ITS which also corrects the aberrations produced by the cornea.

There was also examination of the decentration of the lenses of the ITS. This was done because in the case of a non-functional macula, the image has to be projected at a healthy region of the peripheral retina. The decentration of the image is provided by a prism effect produced from the decentration of the two lenses. The anterior lens of each ITS was decentered with steps of 0.2 mm, up to 1 mm in total. Thus, the image was projected to another part of the retina which is healthy. The decentration was done for both optimized and non-optimized systems. We selected to decenter the lens on one direction only (y axis), because our study was based on a rotationally symmetric eye model. In a customized model (with astigmatism and decentered surfaces in general) the direction of the decentration has to be chosen according to the astigmatism and the retinal area that the image has to be projected. In figure 6.3 and figure 6.4 are shown the designs of the decentered ITS 1 and 2 respectively.

(figure available in printed version)

Figure 6.3 *ITS 1 with decentered anterior lens. a. cornea, b. anterior positive lens, c. pupil, d. posterior negative lens, e. retina.*

(figure available in printed version)

Figure 6.4 *ITS 2 with decentered anterior lens. a. cornea, b. pupil, c. anterior positive lens, d. posterior positive lens, e. retina.*

In order to be able to decenter the lenses in the ray tracing sofware, there were two more surfaces added on the surfaces of each lens. These surfaces are called Coordinate break surfaces and they actually help the user to decenter the lens from the optical axis[67]. They do not alter in any way the final results of optical and visual quality; they only serve as a tool for changing the position of each lens.

After performing ray tracing through the optical design program, results were collected in terms of wavefront RMS error and Zernike coefficients in text files generated from the optical design program. These results were fed into a custom made program in Matlab which calculates the VSOTF [69, 70]. It is considered to be one of the best metrics for assessing retinal image quality and has been used in many research studies. It is calculated as a ratio of the system's integrated optical transfer function modulated by the contrast sensitivity function to its equivalent for a diffraction-limited system,

$$VSOTF = \frac{\int_{-\infty}^{\infty}\int_{-\infty}^{\infty} CSF_N(f_x,f_y)*OTF(f_x,f_y)df_xdf_y}{\int_{-\infty}^{\infty}\int_{-\infty}^{\infty} CSF_N(f_x,f_y)*OTF_{DL}(f_x,f_y)df_xdf_y},$$

where $OTF(f_x, f_y)$ represents the optical transfer function, $OTF_{DL}(f_x, f_y)$ represents the diffraction-limited optical transfer function, $CSF_N(f_x, f_y)$ is the neural contrast sensitivity function, and (f_x, f_y) are the spatial frequency coordinates[70].

The program uses as input the wavefront function which is produced from the optics of the model eye, the telescope and the pupil function that we implement in the ray tracing sofware (circular with 3 mm diameter). By combining these, it calculates the pupil function which, after Fourier transforming, provides the point-spread function. A secondary Fourier transform yields the OTF of the system. The program also calculates the diffraction limited OTF (OTF_{DL}) and the neural contrast sensitivity function (CSF_N) of the system[71]. Finally, it

combines the OTF, OTF_{DL} and CSF_N in order to calculate the VSOTF of the system. Figure 6.5 provides a graphical approach of the algorithm.

(figure available in printed version)

Figure 6.5 *A schematic of the custom algorithm written in Matlab.*

Results

With the previously described procedure, results were gathered for the optical and visual quality of both eye models with the designed ITS. The optical quality was measured in terms of total wavefront RMS error (in wavelengths of 587.6 nm) and the visual quality in terms of VSOTF metric. Results for both optimized and non-optimized telescopic systems were gathered, with either centered or decentered lenses in order to compare them and study the impact of decentration in the quality of vision.

Tables 6.1 and 6.2 show the results for the first and second telescopic systems focused at far target distance, respectively.

Table 6.1 *Optical and Visual results for the first telescopic system (target distance far).*

	Optimized system		Non-optimized system	
Decentration (mm)	RMS (wavelengths)	VSOTF	RMS (wavelengths)	VSOTF
0.0	0.00017	0.99997	0.06621	0.67655
0.2	0.04750	0.56845	0.12529	0.24763
0.4	0.11107	0.27600	0.25315	0.09752
0.6	0.20162	0.19473	0.44053	0.07813
0.8	0.32587	0.17874	0.69565	0.10008
1.0	0.48908	0.18612	1.02587	0.10115

Table 6.2 *Optical and Visual results for the second telescopic system (target distance far).*

	Optimized system		Non-optimized system	
Decentration (mm)	RMS (wavelengths)	VSOTF	RMS (wavelengths)	VSOTF
0.0	0.00032	0.99997	0.04573	0.80058
0.2	0.04446	0.65255	0.10011	0.25081
0.4	0.12208	0.40203	0.25297	0.11908
0.6	0.24940	0.37397	0.51092	0.14969
0.8	0.43805	0.32400	0.88700	0.16121
1.0	0.70249	0.09259	1.40018	0.00757

In figure 6.6 are graphically represented the optical quality results for far target distance in terms of wavefront RMS error. The wavefront RMS error results were calculated through the ray tracing procedure of the ray tracing sofware and they were measured in wavelengths of 587.6 nm. Figure 6.6 also shows the visual quality results for far target distance in terms of the visual Strehl ratio metric.

(figure available in printed version)

Figure 6.6 *Telescope root mean square (RMS) wavefront error (top) and visual Strehl ratio (VSOTF) (bottom) versus decentration of the anterior lens.*

The VSOTF results were calculated through Matlab, through a pupil of 3 mm diameter. Tables 6.3 and 6.4 show the results for the first and second telescopic systems focused at near target distance, respectively.

Table 6.3 *Optical and Visual results for the first telescopic system (target distance near).*

	Optimized system		Non-optimized system	
Decentration (mm)	RMS (wavelengths)	VSOTF	RMS (wavelengths)	VSOTF
0.0	0.00050	0.99997	0.08162	0.51337
0.2	0.03162	0.75714	0.13343	0.20787
0.4	0.07285	0.42921	0.25653	0.07948
0.6	0.13094	0.29042	0.44222	0.05522
0.8	0.21107	0.23356	0.69713	0.07219
1.0	0.31791	0.21931	1.02795	0.09214

Table 6.4 *Optical and Visual results for the second telescopic system (target distance near).*

	Optimized system		Non-optimized system	
Decentration (mm)	RMS (wavelengths)	VSOTF	RMS (wavelengths)	VSOTF
0.0	0.00058	0.99997	0.06363	0.64374
0.2	0.03885	0.71124	0.12556	0.17792
0.4	0.10720	0.44347	0.30485	0.07998
0.6	0.22132	0.39109	0.60986	0.09826
0.8	0.39469	0.37503	1.05769	0.14287
1.0	0.64508	0.17847	1.67465	0.00579

In figure 6.7 are shown graphically the optical and visual results for both telescopic systems focused at a near target distance.

(figure available in printed version)

Figure 6.7 *Telescope root mean square (RMS) wavefront error (top) and Strehl ratio (VSOTF) (bottom) versus decentration of the anterior lens for near target distance.*

When the lenses of each ITS were decentered, the image was also moving towards the peripheral area of the fovea. This image decentration was also measured in the ray tracing sofware and the results for the non-optimized ITS are shown in table 6.5. In table 6.6 are gathered the results for the optimized ITS image decentration for far and near target distances.

Table 6.5 *Image decentration for non-optimized ITS over anterior lens decentration.*

	ITS 1 (non-optimized)		ITS 2 (non-optimized)	
Anterior lens decentration (mm)	Image decentration for far target distance (mm)	Image decentration for near target distance (mm)	Image decentration for far target distance (mm)	Image decentration for near target distance (mm)
0.2	0.1953	0.1991	0.2082	0.2152
0.4	0.4016	0.3992	0.4222	0.4240
0.6	0.6010	0.6017	0.6278	0.6440
0.8	0.7952	0.7992	0.8346	0.8585
1.0	1.0130	1.0020	1.0610	*1.0810*

Table 6.6 *Image decentration for optimized ITS over anterior lens decentration.*

	ITS 1 (optimized)		ITS 2 (optimized)	
Anterior lens decentration (mm)	Image decentration for far target distance (mm)	Image decentration for near target distance (mm)	Image decentration for far target distance (mm)	Image decentration for near target distance (mm)
0.2	0.1953	0.2041	0.2110	0.2179
0.4	0.4037	0.3992	0.4227	0.4324
0.6	0.6051	0.6042	0.6304	0.6440
0.8	0.7964	0.8042	0.8612	0.8585
1.0	0.9876	1.0020	1.0780	1.0880

Discussion

In AMD there is no central field of vision because the region of the macula is not functional. Due to this pathology, a telescopic system that magnifies and projects the image to a healthy part of the retina is needed. In this study two different ITS were compared. The first one is composed by an anterior lens of +53 D optical power, positioned in front of the pupil and a posterior lens of -64 D optical power, placed behind the pupil. The second telescope is totally positioned behind the pupil and is composed of an anterior lens with optical power +66 D and a posterior lens of -66 D. The target distance was set either at infinity (far target distance, larger than 6 m) or at close reading distance (near target distance, at 0.410 m). In order to focus on different target distances, the distance between the lenses has to change as well in both telescopes. For the first telescope focused at far target distance, the lens distance was 3.1 mm, while for near target distance the lens distance increased at 3.65 mm. For the second telescope focused at far target distance, the lens distance was 1.5 mm, while for near target distance the lens distance increased at 1.95 mm.

For both telescopes (see figure 6.6) the optical and visual quality is better when the lenses are aspheric in order to correct the aberrations induced by the cornea and the implantation procedure. ITS 1 provides better optical and visual results than ITS 1. The same observations can be done from figures 6.4 and 6.5 for the near target distance results. Both ITS could provide equal quality of vision in AMD patients. The ITS 2 provides slightly better

results and the fact the whole ITS is behind the pupil and is smaller in length, makes it a better option. This doesn't mean that the ITS 1 design is not a good choice. Another parameter that plays a significant role in the choice of an ITS is the axial length of the eye. As Felipe et al[82] stated in their study, longer eyes (myopic) are more suitable for the ITS 1.

A further expansion of this study could be considered in order to optimize the asphericities of the anterior lens after the decentration of the lens. This could result in better optical and visual quality and it was done in the study of Tabernero et al.[84] In this study the optimization was done before the decentration of the lenses in order to test the image quality when the doctor has to select the decentration of an already manufactured ITS.

For the near target images, the results follow the same trend with the ones for the far target (figure 6.7). The VSOTF decreases as the decentration increases. Nevertheless, between 0.4 and 0.8 mm of decentration the difference between the results is not large. This could indicate a field of decentrations that a surgeon free to choose. In this way, possibly he could choose the part of the retina he wants to target knowing that the provided quality will be more or less the same.

In general, while the decentration increases, the quality decreases dramatically. There are astigmatic and coma aberrations induced because of the decentration of the lenses. As Tabernero et al[84] propose in their study, a cylinder lens could be used in order to fix the induced astigmatism. On the other hand, between 0.4 and 0.8 mm of decentration, the final image quality doesn't change that much, either for far or for near target distances. For these decentrations the retinal image is decentered between 0.4 and 0.8 mm (tables 6.5 and 6.6). This decentration is within the central 3.5 degrees of the retina, which is the foveal and parafoveal area. Depending on the damage of the retina, the surgeon can choose a specific decentration for each patient, keeping in mind that the quality of the image will not change that much. Especially for ITS 2 the calculated VSOTF is above the 0.3 limit that represents the 0 logMAR, as it is proposed from Cheng et al[72]. Of course the image is decentered to a retinal region that does not provide high quality of vision, so the final visual result might be even smaller, but the optical quality provided by the ITS is better than the visual quality that the brain can obtain from that region of the retina.

Finally, a biometric check could be a helpful tool in order to choose which of the two systems might be a better solution. From optical and visual quality both ITS provide the

same quality of image. The decentration of the lenses of the ITS decreases the optical and visual quality. On the other hand, between 0.4 and 0.8 mm, the quality is not decreasing a lot, so the doctor has a decentration field to choose in order to target a precise target area of the retina, near the fovea. In this way, there could be a better optimization of the ITS for each patient depending to his biometric data and the damage of the retina.

Chapter 7.
Conclusions and future work

In this Thesis the optical impact of the correcting elements was studied. Correcting elements such as IOLs and CLs were designed in an optical design program. These elements were designed into theoretical eye models that were also designed in the same program.

The optical impact of these elements is actually the results that these elements induce into the optical system of the human eye. After simulating the theoretical eye models with and without correcting elements, the optical impact was assessed in terms of optical and visual quality. The optical quality was evaluated in terms of wavefront RMS error. There were also collected and studied the Zernike coefficients of this wavefront analysis. The visual quality was evaluated in terms of the visual Strehl ratio based on the OTF of the optical system of the theoretical human eye model with the correcting elements.

The conclusions and the outcomes from this Thesis are collected and presented below:

The optical quality is different from the visual quality in a theoretical human eye model. The optical quality evaluates the quality of the image that is projected on the retina. The visual quality evaluates the quality of the image that is collected from the brain and has to include other parameters except from the refraction of the image. Parameters like the pupil function, the contrast sensitivity function and the OTF.

There is no perfect theoretical human eye model. There is a variety of eye models that include different parameters and are designed with different ways. Each one is built to simulate a human eye but all of them are based on parameter mean values so the simulation is a mean valued human eye model. The decision of using a model in a project is always on the researcher and depends on the research targets.

The dioptric power distribution of a monofocal IOL has to be ~75% of the total power on the anterior surface. The posterior surface has to carry the remaining power. The asphericities of the IOL have to be designed on the anterior surface of the IOL for better optical quality. If they have to be designed on the posterior surface, then, more asphericity orders are needed in order to increase the optical quality.

Optimized and robust (non-optimized) monofocal IOLs provide different optical and visual quality results but the difference is not clinically significant. A combination of an IOL and a CL offers improved optical and visual quality. Misalignments (such as decentrations and tilts) decrease the optical and visual quality results when only an IOL is used. The combination of an IOL and a CL offers increased tolerance to misalignments.

Diffractive multifocal IOLs can be designed and simulated in optical design programs. Optimized and robust (non-optimized) IOLs provide different optical and visual quality results but the difference is not clinically significant. Far vision quality is better than near vision, which is strongly affected from the diffraction of the light on the diffraction pattern of the IOL. Misalignments affect strongly the optical and visual quality provided by the diffractive IOL and have to be restricted in small magnitudes.

Double IOL magnification devices can provide some acceptable optical and visual quality results to patients with low vision. There is an area of decentrations that can be used in order to decenter the image projected to the retina, while the provided quality is not decreasing too much.

Some future work that could be done in this field in continuation of this Thesis:

- Use of more complicated eye models and polychromatic simulations, with or without correcting elements.
- Designs and simulations of specific correcting element designs from patents that could be improved.
- Further designs and simulations on diffractive multifocal IOL from patents, bifocal and trifocal.
- Simulations of refractive multifocal IOLs and comparison studies with diffractive IOLs.
- Studies based on personalized eye models with more biometric data and multifocal IOLs, either diffractive or refractive.
- Comparative studies between simulations and clinical results from real subjects.
- Multifocal CL designs that could be also improved or creation of new designs.

Such studies could lead in advanced depth of focus for these correcting elements and improved optical quality of the projected retinal image.

Bibliography

1 Remington LA. *Clinical anatomy of the visual system*. Elsevier Health Sciences; 2011.
2 M. Yanoff JSD. *Ophthalmology*. 4th. Canada: Elsevier; 2013.
3 Von Helmholtz H. *Handbuch der physiologischen Optik*. Voss; 1867.
4 Pallikaris IG, Plainis S, Charman WN. *Presbyopia: Origins, Effects, and Treatment*. Slack Incorporated New Jersey; 2012.
5 Ophthalmology AAO. Theories of Accommodation. Accessed on 21 October, 2016. Link: http://www.aao.org/bcscsnippetdetail.aspx?id=f5f61688-98cd-4e30-84c0-b9acf775950c
6 Fisher R. Presbyopia and the changes with age in the human crystalline lens. *The Journal of Physiology* 1973;3 (228): 765
7 Glasser A, Campbell MC. Presbyopia and the optical changes in the human crystalline lens with age. *Vision Research* 1998;2 (38): 209-229
8 Schachar RA, Tello C, Cudmore DP, Liebmann JM, Black TD, Ritch R. In vivo increase of the human lens equatorial diameter during accommodation. *American Journal of Physiology-Regulatory, Integrative and Comparative Physiology* 1996;3 (271): R670-R676
9 García-Lázaro S, Ferrer-Blasco T, Radhakrishnan H, Albarrán-Diego C, Montés-Micó R. Visual comparison of an artificial pupil contact lens to monovision. *Optometry & Vision Science* 2012;7 (89): E1022-E1029
10 Luger MHA, Ewering T, Arba-Mosquera S. One-Year Experience in Presbyopia Correction With Biaspheric Multifocal Central Presbyopia Laser In Situ Keratomileusis. *Cornea* 2013;5 (32): 644-652
11 Kim P, Sutton GL, Rootman DS. Applications of the femtosecond laser in corneal refractive surgery. *Current Opinion in Ophthalmology* 2011;4 (22): 238-244
12 Lindstrom RL, Macrae SM, Pepose JS, Hoopes PC, Sr. Corneal inlays for presbyopia correction. *Current Opinion in Ophthalmology* 2013;4 (24): 281-287
13 Kim TJ. Presbyopia and contact lenses. *Journal of the Korean Medical Association/Taehan Uisa Hyophoe Chi* 2013;4 (56)
14 Lichtinger A, Rootman DS. Intraocular lenses for presbyopia correction: past, present, and future. *Current Opinion in Ophthalmology* 2012;1 (23): 40-46
15 Navarro R. The Optical Design of the Human Eye: a Critical Review. *Journal of Optometry* 2009;1 (2): 3-18
16 Navarro R, Santamaría J, Bescós J. Accommodation-dependent model of the human eye with aspherics. *Journal of the Optical Society of America A* 1985;8 (2): 1273-1280
17 Liou H-L, Brennan NA. Anatomically accurate, finite model eye for optical modeling. *Journal of the Optical Society of America A* 1997;8 (14): 1684-1695
18 Schwiegerling J. *Field Guide to Visual and Ophthalmic Optics*. SPIE Publications; 2004.
19 Rozema JJ, Atchison DA, Tassignon M-J. Statistical Eye Model for Normal Eyes. *Investigative Ophthalmology & Visual Science* 2011;7 (52): 4525-4533
20 Atchison D, Smith G. *Optics of the human eye*. Oxford: Elsevier Health Sciences; 2000.
21 Andrade de Jesus D, Iskander DR. Numerical simplification of ray tracing for non-circularly symmetric models of the human eye. *Investigative Ophthalmology & Visual Science* 2015;7 (56): 6018-6018
22 Polans J, Jaeken B, McNabb RP, Hervella L, Artal P, Izatt JA. Wide-field schematic model of the Human Eye with Asymmetrically Tilted and Decentered Lens. *Investigative Ophthalmology & Visual Science* 2015;7 (56): 6019-6019

23 Artal P, Benito A, Tabernero J. The human eye is an example of robust optical design. *Journal of Vision* 2006;1 (6): 1-1

24 Navarro R. Adaptive model of the aging emmetropic eye and its changes with accommodation. *Journal of Vision* 2014;13 (14): 21

25 Goldberg DB. Computer-animated model of accommodation and presbyopia. *Journal of Cataract and Refractive Surgery* 2015;2 (41): 437-445

26 Reilly MA. A quantitative geometric mechanics lens model: insights into the mechanisms of accommodation and presbyopia. *Vision Research* 2014;(103): 20-31

27 Van de Sompel D, Kunkel GJ, Hersh PS, Smits AJ. Model of accommodation: contributions of lens geometry and mechanical properties to the development of presbyopia. *Journal of Cataract and Refractive Surgery* 2010;11 (36): 1960-1971

28 Lanchares E, Navarro R, Calvo B. Hyperelastic modelling of the crystalline lens: Accommodation and presbyopia. *Journal of Optometry* 2012;3 (5): 110-120

29 Richdale K, Sinnott LT, Bullimore MA, Wassenaar PA, Schmalbrock P, Kao C-Y, Patz S, Mutti DO, Glasser A, Zadnik K. Quantification of Age-Related and per Diopter Accommodative Changes of the Lens and Ciliary Muscle in the Emmetropic Human EyeLens and Ciliary Muscle with Age and Accommodation. *Investigative Ophthalmology & Visual Science* 2013;2 (54): 1095-1105

30 Huang JY, Moore D. Computer simulated human eye modeling with GRIN incorporated in the crystalline lens. *Journal of Vision* 2004;11 (4): 58-58

31 Gambra E, Ortiz S, Perez-Merino P, Gora M, Wojtkowski M, Marcos S. Static and dynamic crystalline lens accommodation evaluated using quantitative 3-D OCT. *Biomedical Optics Express* 2013;9 (4): 1595-1609

32 Zhong J, Tao A, Xu Z, Jiang H, Shao Y, Zhang H, Liu C, Wang J. Whole eye axial biometry during accommodation using ultra-long scan depth optical coherence tomography. *American Journal of Ophthalmology* 2014;5 (157): 1064-1069

33 Kasthurirangan S, Markwell EL, Atchison DA, Pope JM. MRI study of the changes in crystalline lens shape with accommodation and aging in humans. *Journal of Vision* 2011;3 (11)

34 Charman WN. The eye in focus: accommodation and presbyopia. *Clinical and Experimental Optometry* 2008;3 (91): 207-225

35 Rosales P, Dubbelman M, Marcos S, van der Heijde R. Crystalline lens radii of curvature from Purkinje and Scheimpflug imaging. *Journal of Vision* 2006;10 (6): 5-5

36 Dubbelman M, Van der Heijde GL, Weeber HA. Change in shape of the aging human crystalline lens with accommodation. *Vision Research* 2005;1 (45): 117-132

37 Kasthurirangan S, Markwell EL, Atchison DA, Pope JM. MRI study of the changes in crystalline lens shape with accommodation and aging in humans. *Journal of Vision* 2011;3 (11): 19-19

38 Fischer R, Tadic-Galeb B. *Optical System Design*. Second Edition. New York: The McGraw-Hill Companies, Inc.; 2008.

39 Smith WJ. *Modern Optical Engineering: The Design of Optical Systems*. Third Edition. New York: The McGraw-Hill Companies, Inc.; 2000.

40 Read SA, Collins MJ, Woodman EC, Cheong S-H. Axial Length Changes During Accommodation in Myopes and Emmetropes. *Optometry & Vision Science* 2010;9 (87): 656-662

41 Almeida MSd, Carvalho LA. Different schematic eyes and their accuracy to the in vivo eye: a quantitative comparison study. *Brazilian Journal of Physics* 2007;2 (37): 378-387

42 Koretz JF, Cook CA, Kaufman PL. Accommodation and presbyopia in the human eye - Changes in the anterior segment and crystalline lens with focus. *Investigative Ophthalmology and Visual Science* 1997;3 (38): 569-578
43 Allen D, Vasavada A. Cataract and surgery for cataract. *British Medical Journal* 2006(7559): 128
44 Leyland M, Zinicola E. Multifocal versus monofocal intraocular lenses in cataract surgery: A systematic review. *Ophthalmology* 2003;9 (110): 1789-1798
45 Madrid-Costa D, Ruiz-Alcocer J, Ferrer-Blasco T, Garcia-Lazaro S, Montes-Mico R. Optical quality differences between three multifocal intraocular lenses: bifocal low add, bifocal moderate add, and trifocal. *Journal of refractive surgery* 2013;11 (29): 749-754
46 Ruiz-Alcocer J, Madrid-Costa D, Garcia-Lazaro S, Ferrer-Blasco T, Montes-Mico R. Optical performance of two new trifocal intraocular lenses: through-focus modulation transfer function and influence of pupil size. *Clinical & Experimental Ophthalmology* 2014;3 (42): 271-276
47 Olsen T. Calculation of intraocular lens power: a review. *Acta Ophthalmologica Scandinavica* 2007;5 (85): 472-485
48 Schuster AK, Tesarz J, Vossmerbaeumer U. The impact on vision of aspheric to spherical monofocal intraocular lenses in cataract surgery: a systematic review with meta-analysis. *Ophthalmology* 2013;11 (120): 2166-2175
49 Zemax. Zemax webpage. Accessed on 1 October 2016, 2014. Link: https://www.zemax.com/
50 Eppig T, Scholz K, Löffler A, Meßner A, Langenbucher A. Effect of decentration and tilt on the image quality of aspheric intraocular lens designs in a model eye. *Journal of Cataract & Refractive Surgery* 2009;6 (35): 1091-1100
51 Wang L, Koch DD. Custom optimization of intraocular lens asphericity. *Journal of Cataract & Refractive Surgery* 2007;10 (33): 1713-1720
52 Canovas C, Artal P. Customized eye models for determining optimized intraocular lenses power. *Biomedical Optics Express* 2011;6 (2): 1649-1662
53 Bellucci R, Morselli S. Optimizing higher-order aberrations with intraocular lens technology. *Current Opinion in Ophthalmology* 2007;1 (18): 67-73
54 Kozaki J, Takahashi F. Theoretical analysis of image defocus with intraocular lens decentration. *Journal of Cataract & Refractive Surgery* 1995;5 (21): 552-555
55 Taketani F, Matuura T, Yukawa E, Hara Y. Influence of intraocular lens tilt and decentration on wavefront aberrations. *Journal of Cataract & Refractive Surgery* 2004;10 (30): 2158-2162
56 Murphy C, Tuft SJ, Minassian DC. Refractive error and visual outcome after cataract extraction. *Journal of Cataract & Refractive Surgery* 2002;1 (28): 62-66
57 Gale RP, Saldana M, Johnston RL, Zuberbuhler B, McKibbin M. Benchmark standards for refractive outcomes after NHS cataract surgery. *Eye* 2007;1 (23): 149-152
58 de Vries NE, Webers CAB, Touwslager WRH, Bauer NJC, de Brabander J, Berendschot TT, Nuijts RMMA. Dissatisfaction after implantation of multifocal intraocular lenses. *Journal of Cataract & Refractive Surgery* 2011;5 (37): 859-865
59 Mamalis N, Crandall AS, Pulsipher MW, Follett S, Monson MC. Intraocular lens explantation and exchange. A review of lens styles, clinical indications, clinical results, and visual outcome. *Journal of Cataract & Refractive Surgery* 1991;6 (17): 811-818

60 Fernandez-Buenaga R, Alio JL, Perez Ardoy AL, Quesada AL, Pinilla-Cortes L, Barraquer RI. Resolving refractive error after cataract surgery: IOL exchange, piggyback lens, or LASIK. *Journal of Refractive Surgery* 2013;10 (29): 676-683

61 Ayala MJ, Perez-Santonja JJ, Artola A, Claramonte P, Alio JL. Laser in situ keratomileusis to correct residual myopia after cataract surgery. *Journal of Refractive Surgery* 2001;1 (17): 12-16

62 Sáles CS, Manche EE. Managing residual refractive error after cataract surgery. *Journal of Cataract & Refractive Surgery* 2015;6 (41): 1289-1299

63 McKelvie J, McArdle B, McGhee C. The influence of tilt, decentration, and pupil size on the higher-order aberration profile of aspheric intraocular lenses. *Ophthalmology* 2011;9 (118): 1724-1731

64 Guo H, Goncharov AV, Dainty C. Comparison of retinal image quality with spherical and customized aspheric intraocular lenses. *Biomedical Optics Express* 2012;4 (3): 681-691

65 Rozema JJ, Atchison DA, Tassignon MJ. Statistical eye model for normal eyes. *Investigative Ophthalmology & Visual Science* 2011;7 (52): 4525-4533

66 Iskander DR, Collins MJ, Davis B. Optimal modeling of corneal surfaces with Zernike polynomials. *Biomedical Engineering, IEEE Transactions on* 2001;1 (48): 87-95

67 *Zemax Optical Design Program User's Guide*. 2005.

68 Bhardwaj V, Rajeshbhai GP. Axial Length, Anterior Chamber Depth-A Study in Different Age Groups and Refractive Errors. *Journal of Clinical and Diagnostic Research* 2013;10 (7): 2211-2212

69 Marsack JD, Thibos LN, Applegate RA. Metrics of optical quality derived from wave aberrations predict visual performance. *Journal of Vision* 2004;4 (4): 8-8

70 Iskander DR. Computational Aspects of the Visual Strehl Ratio. *Optometry & Vision Science* 2006;1 (83): 57-59

71 Campbell FW, Green DG. Optical and retinal factors affecting visual resolution. *The Journal of Physiology* 1965;3 (181): 576-593

72 Cheng X, Bradley A, Thibos LN. Predicting subjective judgment of best focus with objective image quality metrics. *Journal of Vision* 2004;4 (4): 310-321

73 Polans J, Jaeken B, McNabb RP, Artal P, Izatt JA. Wide-field optical model of the human eye with asymmetrically tilted and decentered lens that reproduces measured ocular aberrations. *Optica* 2015;2 (2): 124-134

74 Atchison DA, Thibos LN. Optical models of the human eye. *Clinical and Experimental Optometry* 2016;2 (99): 99-106

75 Jager RD, Mieler WF, Miller JW. Age-Related Macular Degeneration. *New England Journal of Medicine* 2008;24 (358): 2606-2617

76 Lim LS, Mitchell P, Seddon JM, Holz FG, Wong TY. Age-related macular degeneration. *The Lancet* 2012;9827 (379): 1728-1738

77 Cook HL, Patel PJ, Tufail A. Age-related macular degeneration: diagnosis and management. *British Medical Bulletin* 2008;1 (85): 127-149

78 Qureshi MA, Robbie SJ, Tabernero J, Artal P. Injectable intraocular telescope: Pilot study. *Journal of Cataract & Refractive Surgery* 2015;10 (41): 2125-2135

79 Hudson HL, Stulting RD, Heier JS, Lane SS, Chang DF, Singerman LJ, Bradford CA, Leonard RE, Group IS. Implantable telescope for end-stage age-related macular degeneration: long-term visual acuity and safety outcomes. *American Journal of Ophthalmology* 2008;5 (146): 664-673. e661

80 Singer MA, Amir N, Herro A, Porbandarwalla SS, Pollard J. Improving quality of life in patients with end-stage age-related macular degeneration: focus on miniature ocular implants. *Clinical Ophthalmology* 2012(6): 33-39

81 Lane SS, Kuppermann BD. The implantable miniature telescope for macular degeneration. *Current Opinion in Ophthalmology* 2006;1 (17): 94-98

82 Felipe A, Díaz-Llopis M, Navea A, Artigas JM. Optical analysis to predict outcomes after implantation of a double intraocular lens magnification device. *Journal of Cataract & Refractive Surgery* 2007;10 (33): 1781-1789

83 Agarwal A, Lipshitz I, Jacob S, Lamba M, Tiwari R, Kumar DA, Agarwal A. Mirror telescopic intraocular lens for age-related macular degeneration: design and preliminary clinical results of the Lipshitz macular implant. *Journal of Cataract & Refractive Surgery* 2008;1 (34): 87-94

84 Tabernero J, Qureshi MA, Robbie SJ, Artal P. An aspheric intraocular telescope for age-related macular degeneration patients. *Biomedical Optics Express* 2015;3 (6): 1010-1020

85 Goncharov AV, Dainty C. Wide-field schematic eye models with gradient-index lens. *Journal of the Optical Society of America A, Optics, image science, and vision* 2007;8 (24): 2157-2174

Appendix A. Matlab code for diffractive multifocal IOLs

In this part of the thesis is presented the custom made Matlab code that was created by Georgios Zoulinakis during his PhD, in University of Valencia. This code was used in order to design spherical, aspherical and diffractive bifocal aspherical IOL surfaces that were used within this manuscript in chapters 3, 4 and 5.

The code is going to be presented in parts and below and `will be written in this font style` in order to be discriminated. Each part will be given an explanation of it. There are also notes in the code that provide more information and directions about how the data should be input by the programmer.

Part 1:

```
%%%%%% Code for designing multifocal diffractive IOLs
%%%%%% This code was created by Georgios Zoulinakis
%%%%%% Fellow member of the AGEYE ITN program, Marie Curie Actions, EU
%%%%%% University of Valencia, Valencia, Spain, 2015 - 2016

%%%%%% Beware of the units, all must be in mm
%%%%%% IOLs with central refractive area

clear all; close all

%%%~~~Diffraction profile
phase=0.5;              %%% phase difference in wavelengths
wavelength=555*10^-6;   %%% wavelength used in simulations in mm
n1=1.337;               %%% refractive index of aqueous
n2=1.55;                %%% refractive index of the IOL
Max_Stepheight=phase*wavelength/(n2-n1);    %%% maximum stepheight of
diffraction profile in mm

Nmax=10;   %%% max number of diffractive zones
max_r=3;   %%% maximum surface distance (radius) of IOL in mm

f_near=500;   %%% focal length of near focus in mm
r_central=1;       %%%%%%%%%% alternatively: sqrt(wavelength*f_near);
%%% radius of central refractive zone,             %%%%%    it    can    be
selected also by user or by the function

for i=1:Nmax   %%% eschellete outer boundary
    eschellete_r(i)=sqrt((r_central^2)+2*i*wavelength*f_near);     %%%
radial coordinations of the eschelette
end
eschellete_r=[r_central  eschellete_r];     %%%  eschellete  boundaries
with central refractive zone

steps=50;                           %%% number of points on r dimension
for each eschellete
internal_steps=50;                    %%% number of points of internal
refractive region
external_steps=80;                   %%% number of points of external
refractive region
r=[];                                     %%% empty surface distance r
coordinate
for i=1:length(eschellete_r)-1
```

```
        r=[r  linspace(eschellete_r(i),eschellete_r(i+1),steps)];       %%%
r_coordinate between the eschelletes
    end
    r=[linspace(0,r_central,internal_steps)                                  r
linspace(eschellete_r(Nmax+1),max_r,external_steps)];    %%% build up of r
coordinate between each step, beware not to exceed r_max
```

Up to this point in the first part the programmer inputs the needed values for the code in order to make the calculations later on. The code calculates and saves the radial coordinates of each diffractive step (eschellete). In the end the code saves in the matrix r a number of radial coordinates that are all the points from the center of the IOL (optical axis) until the edge of the IOL optical part. The number of the points is controlled by the programmer.

Part 2:

```
    %%%~~~Apodization function
    r_in=1;      %%%%%%r_central; inner limit of apodization zone, varies
between 0 and 3 mm, r_in < r_out
    r_out=3;      %%%%%% eschellete_r(Nmax+1); outer limit of apodization
zone, varies between 0 and 3 mm, r_in < r_out
    exp=3;      %%% exponential apodization factor, between 3 - 6
    for i=1:length(r)
        if r(i)<r_in
            f_apod(i)=1;
        elseif r(i)<=r_out
            f_apod(i)=1-((r(i)-r_in)/(r_out-r_in))^exp;    %%% apodization
function, for no apodization in the
                                                          %%%   steps   we
have to replace f_apod=1 everywhere
        else                                                          %%%%%%
Alternative function f_apod=1-(r(i)/r_out)^3
            f_apod(i)=0;
        end
    end

    figure;
    % % % set(gca,'fontsize',24)
    plot(r, f_apod, '.')
    title('Apodization function')
    xlabel('Surface radial coordinate (mm)')
    ylabel('Apodization height factor (no units)')
```

In the second part the code calculates the apodization function matrix (f_apod) that will be applied on the diffraction pattern. This function actually makes each stepheight smaller as the radial coordinate moves from the centre of the IOL (optical axis) to the periphery. The code provides a plot (figure A.1) that shows the apodization function. If the programmer doesn't want to include an apodization factor to the IOL design he has to set

the apodization function equal to 1 (f_apod=1) and to deactivate the "for loop" that calculates the apodization function.

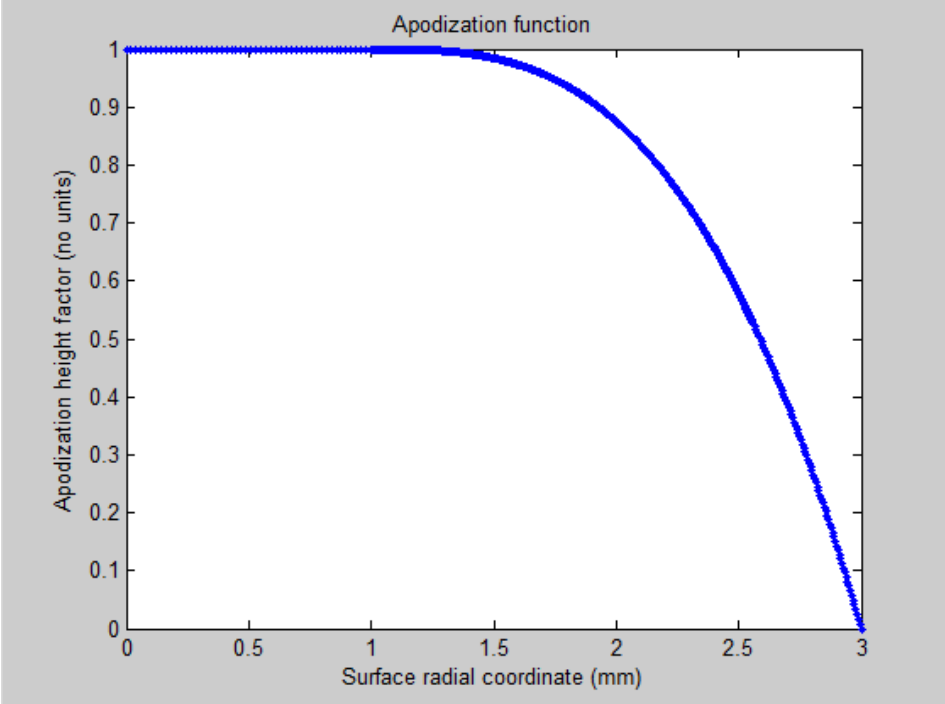

Figure A.1 *Apodization function over the surface radial coordinate.*

Part 3:

```
%%%~~~Apodized diffractive function
N=1;
for i=1:length(r)
    if and(i>internal_steps, N<Nmax)
       dif_sag(i)=Max_Stepheight  *  (1-  (  (r(i)-eschellete_r(N))  /
(eschellete_r(N+1)-eschellete_r(N)) )^2);
        %%% eschellete function %%%~~~sag based at 0
         final_dif_sag(i)=dif_sag(i)-Max_Stepheight/2;         %%%~~~sag
centered at 0
         if dif_sag(i)<=0.0000001                              %%% limit to
be controlled, less than 0.1 nm,
%%% mathematical calculation issue of matlab
           dif_sag(i)=0;                                       %%%~~~sag
based at 0
           final_dif_sag(i)=dif_sag(i)-Max_Stepheight/2;       %%%~~~sag
centered at 0
           N=N+1;
         end
      elseif N==Nmax
       dif_sag(i)=Max_Stepheight  *  (1-  (  (r(i)-eschellete_r(N))  /
(eschellete_r(N+1)-eschellete_r(N)) )^2);
        %%%~~~sag based at 0
         final_dif_sag(i)=dif_sag(i)-Max_Stepheight/2;         %%%~~~sag
centered at 0
         if dif_sag(i)<=0.0000001
             dif_sag(i)=0;                                     %%%~~~sag
based at 0
             final_dif_sag(i)=dif_sag(i)-Max_Stepheight/2;     %%%~~~sag
centered at 0
             N=N+1;
```

```
            end
        else
            dif_sag(i)=0;                   %%%~~~sag based at 0
            final_dif_sag(i)=dif_sag(i);    %%%~~~sag centered at 0
        end                                 %%%~~~sag based at 0
    end
    clear N
    clear i
    figure; plot(r, dif_sag, '.')   %%% Plot of diffractive sag based at 0
    title('Diffraction sag (based at 0)')
    xlabel('Surface radial coordinate (mm)')
    ylabel('Sag height (mm)')
    figure;
    % % % set(gca,'fontsize',24)
    plot(r, final_dif_sag, '.')    %%% Plot of diffractive sag centered at
0
    title('Diffraction sag (centered at 0)')
    xlabel('Surface radial coordinate (mm)')
    ylabel('Sag height (mm)')

    for i=1:length(r)
        final_dif_sag(i)=final_dif_sag(i)*f_apod(i);
    end
    figure;
    % % % set(gca,'fontsize',24)
    plot(r, final_dif_sag, '.')    %%% Plot of the final diffractive sag
    title('Apodized diffraction sag')
    xlabel('Surface radial coordinate (mm)')
    ylabel('Sag height (mm)')
```

In the third part the code actually creates the final apodized diffraction sag matrix (final_dif_sag). It makes all the calculations needed and provides plots (figures A.2 and A.3) with the diffraction pattern either based at 0 line or centered at 0 line (x-axis of the plot). It also provides a plot (figure A.4) of the apodized diffraction pattern centered at 0 line (x-axis).

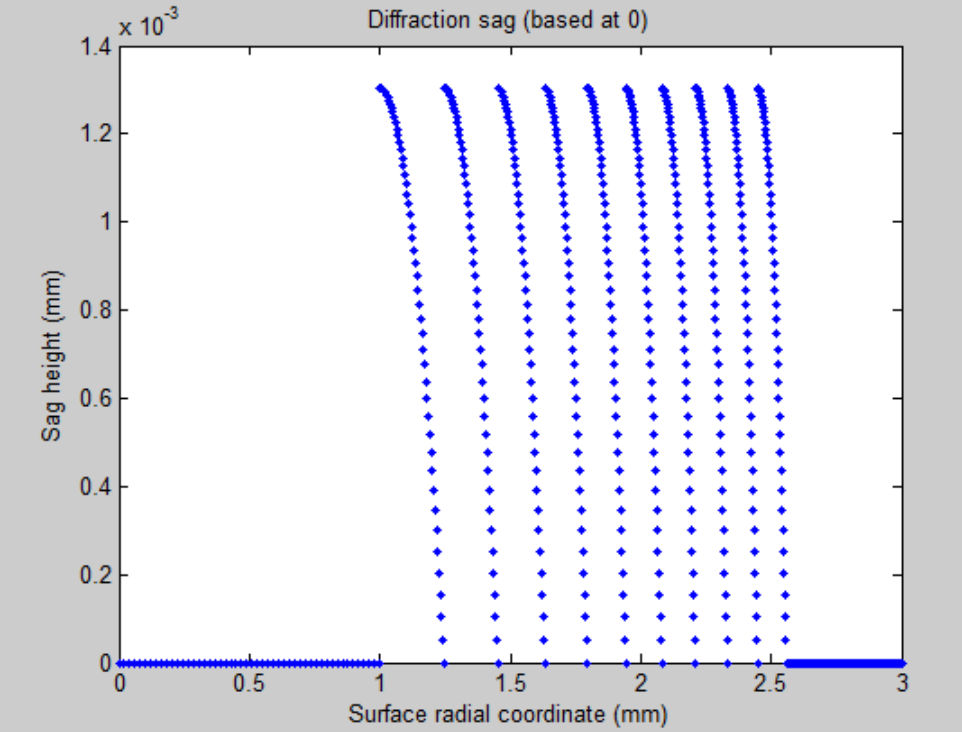

Figure A.2 *Diffraction sag based at 0.*

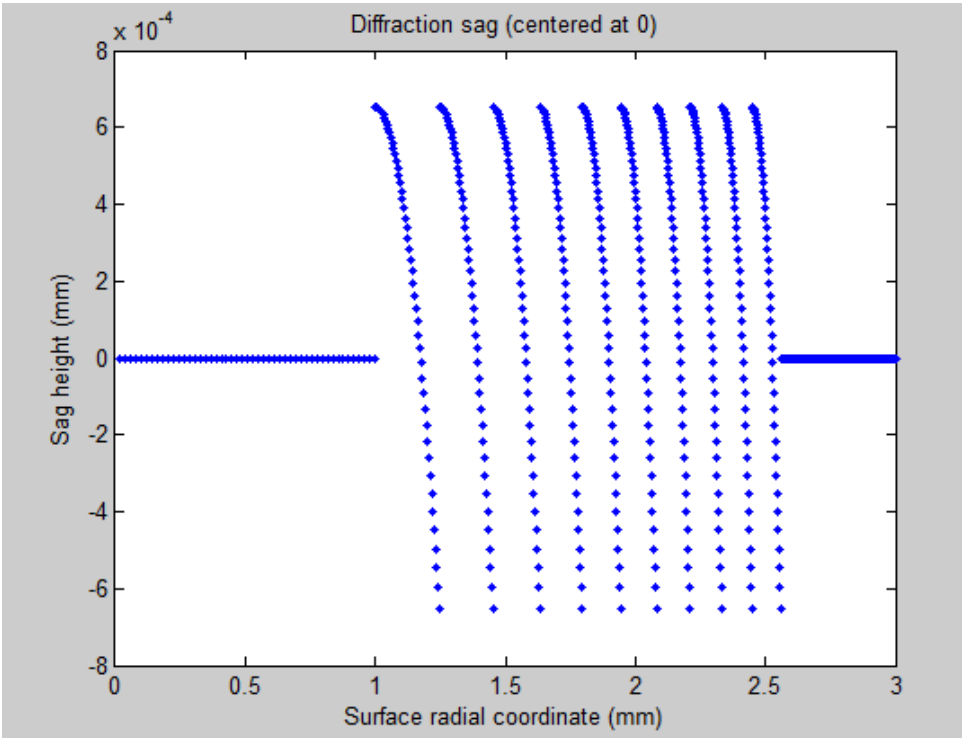

Figure A.3 *Diffraction sag centered at 0.*

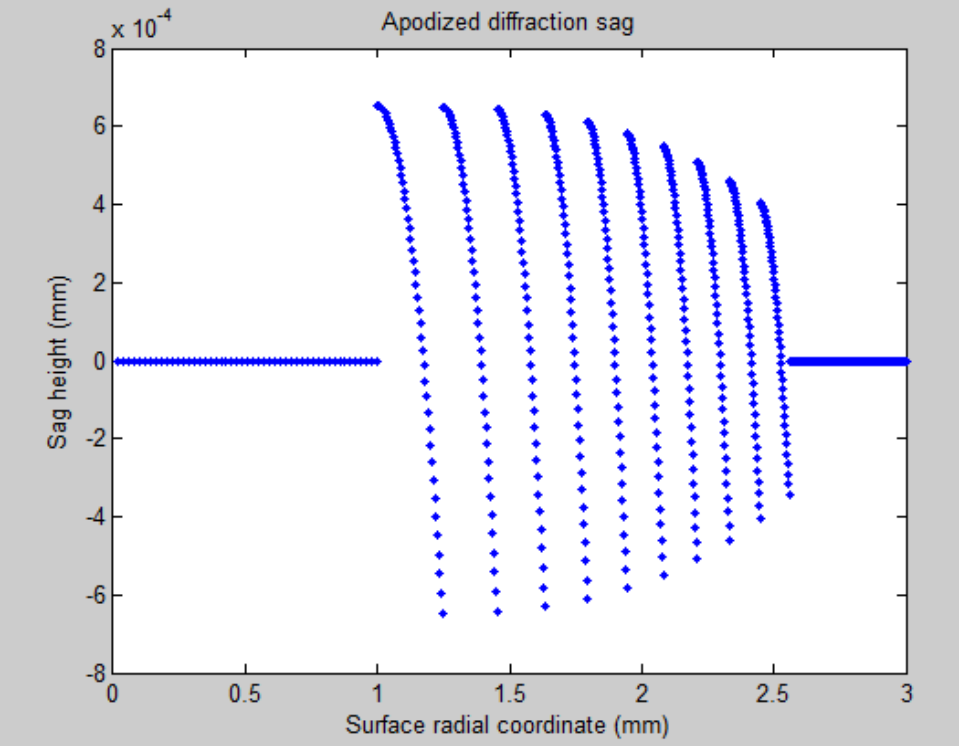

Figure A.4 *Apodized diffraction sag centered at 0.*

Part 4:

```
%%%~~~Spherical sag function with asphericities and conics

R=7.1;                  %%% radius of curvature of spherical sag in mm
cv=1/R;                 %%% curvature
cc=-0.8;                %%% conic constant, range (-1,0)
ac=6.770037*10^-3;      %%% 2nd order aspheric constant
ad=-5.067276*10^-4;     %%% 4th order aspheric constant
ae=0;                   %%% 6th order aspheric constant

Sph_sag=((cv*(r.^2))./(1+sqrt(1-(cv^2)*(cc+1)*r.^2)))   +   ac*r.^2   +
ad*r.^4 + ae*r.^6;      %%% spherical sag in mm, substract from maximum to
have it positive

figure; plot(r, Sph_sag, '.')     %%% Plot of the spherical sag
title('Spherical sag function')
xlabel('Surface radial coordinate (mm)')
ylabel('Sag height (mm)')
```

In the fourth part, the code calculates for the radial coordinates of r, the spherical sag function matrix with all the asphericities up to the 6th order and the conic constant. The programmer has to input all the data for the spherical sag function in this part of the code. The code provides plots of the final spherical or aspherical sag (figure A.5).

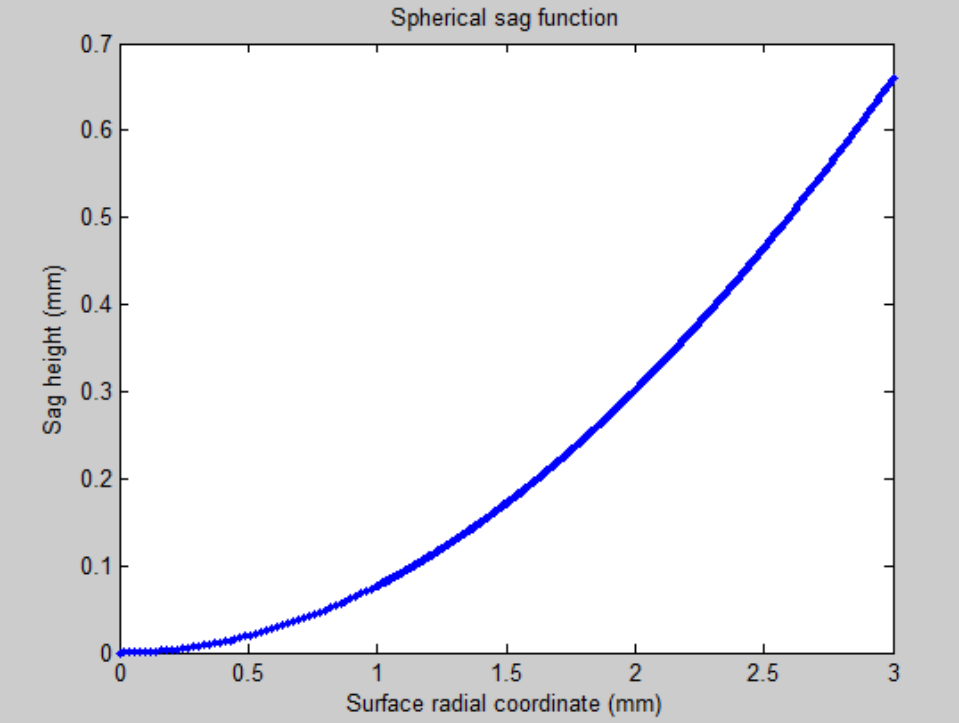

Figure A.5 *Spherical or aspherical sag function.*

Part 5:

```
%%%~~~Total apodized diffractive and spherical sag

Total_IOL_sag=-final_dif_sag+Sph_sag;      %%% negative final_dif_sag
because the sph_sag is up side down
figure; plot(r, Total_IOL_sag, '.')     %%% Plot of the total IOL sag
title('Total IOL sag')
xlabel('Surface radial coordinate (mm)')
ylabel('Sag height (mm)')

%%%~~~Profile turn for the ray tracing software (I use Z at the start
of the names)
figure; plot(Total_IOL_sag, r, '.')      %%% Plot of the total IOL sag
for the ray tracing software
title('Total IOL sag for the ray tracing software')
xlabel('Sag height (mm)')
ylabel('Surface radial coordinate (mm)')

V_Sag_z(1:steps)=max(Total_IOL_sag);              %%% vertical line z
coords
V_Sag_y=linspace(max_r-0.05,0,steps);             %%% vertical line y
coords, different start and finish
                                                  %%% points in order not
to points at the same coordinates
H_lowerSag_z=linspace(max(Total_IOL_sag)-0.005,0,steps);          %%%
horizontal lower line z coords
H_lowerSag_y=zeros(1,steps);                                      %%%
horizontal lower line y coords
```

```
    Y=[r V_Sag_y H_lowerSag_y]';              %%% Y coordinate for the ray
tracing software
    Z=[Total_IOL_sag V_Sag_z H_lowerSag_z]';    %%% Z coordinate for the
ray tracing software

    figure;
    % % % set(gca,'fontsize',24)
    plot(Z, Y, '.')    %%% Plot of the total IOL sag for the ray tracing
software
    title('Total IOL sag for the ray tracing software')
    xlabel('Sag height (mm)')
    ylabel('Surface radial coordinate (mm)')

    disp(sprintf('Surface maximum sag is %s mm',max(Total_IOL_sag)))
%%% maximum sag in order to place the posterior lens in the ray tracing
software

    total_coords=[Y Z];                                  %%% coords in one
matrix
    format short

    %
%%%%~~~~~~~~~~~~~~~~~~~~~~~~~~~~~~~~~~~~~~~~~~~~~~~~~~~~~~~~~~~~~~~~~~~~~~~
    %
    % %%%%%%%%%% save total coordinates Y and Z for the tray tracing
software
    %
    % % % % save 'C:\Users\...\test1.tob' total_coords -ASCII     %%% tob
file for the ray tracing software
    %
    %
%%%%%%%%%%%%%%%%%%%%%%%%%%%%%%%%%%%%%%%%%%%%%%%%%%%%%%%%%%%%%%%%%%%%%%%%%%%
```

In the fifth and last part, the code adds the two sag function matrixes that has calculated before (the final_dif_sag and the Sph_sag) in order to create the final IOL sag matrix (Total_IOL_sag). This is the final cross section of the IOL sag from the optical axis (center of the IOL) up to the edge of the IOL.

After that the code turns the sag to the correct direction (according to the direction of the surface the programmer needs) and adds some additional points on the horizontal and vertical axis (here they are named as z and y, to be the same as the coordination axis in the ray tracing sofware). These points are added because the ray tracing sofware needs these points to design the volume of the lens (it has to be a closed surface). A plot is provided by the code (figure A.6) with the final design. If the zoom option is used in Matlab, the diffraction pattern could be obvious.

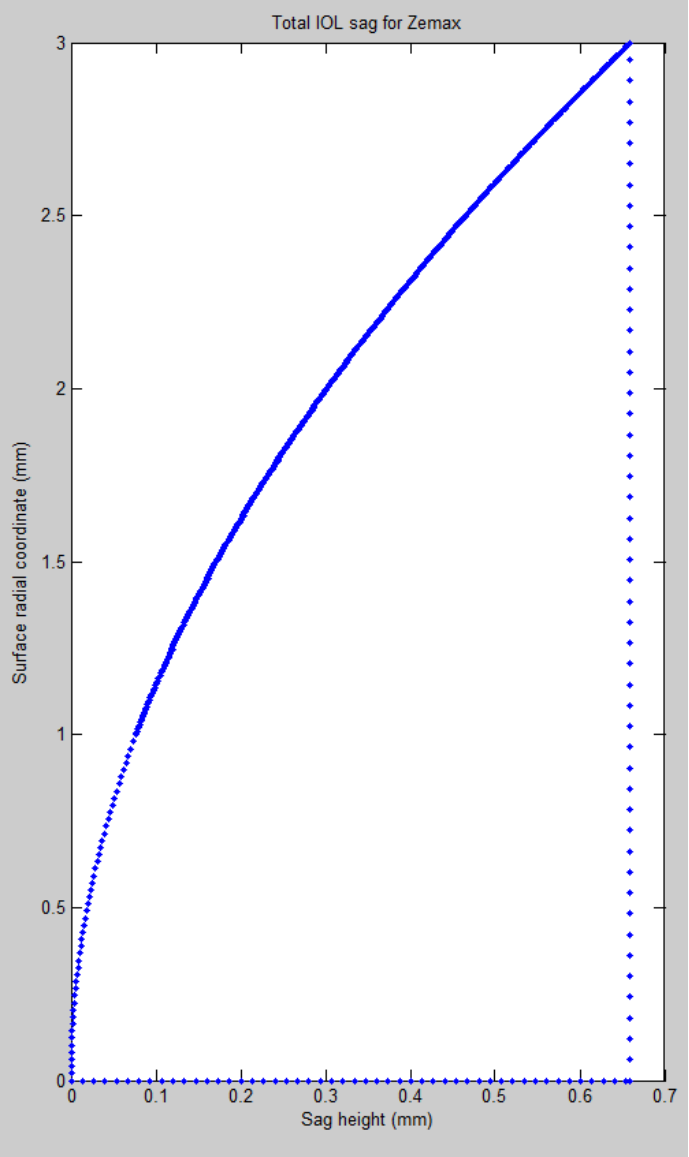

***Figure A.6**. Total IOL sag function with apodized diffraction pattern (not obvious because the stepheights are small).*

In the end the total coordinates of the Total_IOL_sag and the horizontal and vertical points are saved in a text file. This file can then be fed into the optical design program. The program is able to make a revolution of this surface and create a volume, which actually is the anterior diffractive IOL part that the programmer wanted to create. The posterior part of the IOL can be added through the ray tracing sofware.

The code has the possibility to change by deactivating or changing some parts, in order to design negative lenses, or lenses without diffractive patterns. There is also the possibility to add one more part in order to control the function between the steps, instead of spherical can be sinusoidal for example.

Appendix B. Publications and presentations from the Thesis

This PhD Thesis has resulted in the following peer-reviewed publications:

Zoulinakis G, Esteve-Taboada J, Ferrer-Blasco T, Madrid-Costa D, Montés-Micó R. Accommodation in human eye models: a comparison between the optical designs of Navarro, Arizona and Liou-Brennan. Accepted for publication in *International Journal of Ophthalmology.*

Zoulinakis G, Ferrer-Blasco T. Power distribution in monofocal spherical and aspherical intraocular lenses. Submitted for publication (in peer-review process).

Zoulinakis G, Ferrer-Blasco T, Iskander DR. Simulating visual and optic quality of ocular correcting designs. Submitted for publication (in peer-review process).

Zoulinakis G, Ferrer-Blasco T. Intraocular telescopic system design: optical and visual simulation in a human eye model. Submitted for publication (in peer-review process).

Parts of the present Thesis have been presented to the following scientific congresses:

XXXII congress of the European Society of Cataract & Refractive Surgeons (ESCRS), 13-17 September 2014, London, United Kingdom. Comparison of different eye models in simulating healthy and presbyopic eyes. Proceedings of XXXII congress of the ESCRS, abstract book, September 2014. G. Zoulinakis, E. Papadatou, T. Ferrer-Blasco, D. Madrid-Costa, R. Montés-Micó.

OC' 15, Optometry Congress 2015, 7 – 8 March 2015, Valencia, Spain. Design of ocular media and correcting elements and comparison between different eye models. Proceedings of OC'15, March 2015. Zoulinakis G.

XXXIII congress of the European Society of Cataract & Refractive Surgeons (ESCRS), 4-8 September 2015, Barcelona, Spain. Optical power distribution on spherical monofocal intraocular lenses. Proceedings of XXXIII congress of the ESCRS, abstract book, September 2015. Zoulinakis G; Papadatou E; Moulakaki A; Ferrer-Blasco T.

XXXIII congress of the European Society of Cataract & Refractive Surgeons (ESCRS), 4-8 September 2015, Barcelona, Spain. Alternative method for optical design of intraocular lenses. Proceedings of XXXIII congress of the ESCRS, abstract book, September 2015. Zoulinakis G; Moulakaki A; Papadatou E; Ferrer-Blasco T.

The International OSA Network of Student (IONS) congress, Iberian Chapter, 24-26 September 2015, Valencia, Spain. Simulation of diffractive multifocal intraocular lenses (IOLs) with a new designing method. Proceedings of IONS Valencia congress, abstract book, September 2015. Zoulinakis G; Moulakaki A; Papadatou E; Ferrer-Blasco T.

Congreso Internacional de Optometría, Contactología y Óptica Oftálmica (OPTOM) 2016, 8-10 Abril 2016, Madrid, Spain**.** *Un método alternativo para el diseño óptico de lentes intraoculares.* Proceedings of OPTOM congress, abstract book, April 2016. Zoulinakis G; Moulakaki A; Papadatou E; Esteve-Taboada JJ; Ferrer-Blasco T.

Congreso Internacional de Optometría, Contactología y Óptica Oftálmica (OPTOM) 2016, 8-10 Abril 2016, Madrid, Spain**.** *Distribución de potencia óptica en lentes intraoculares monofocales esféricas.* Proceedings of OPTOM congress, abstract book, April 2016. Zoulinakis G; Papadatou E; Moulakaki A; Esteve-Taboada JJ; Ferrer-Blasco T.

The Association for Research in Vision and Ophthalmology (ARVO) Annual Meeting, 1-5 May, 2016, Seattle, Washington, USA. Visual quality with combinations of optimized and non-optimized corrective elements. Proceedings of ARVO Annual Meeting, abstract book, May 2016. Zoulinakis G; Montes-Mico R; Ferrer-Blasco T; Iskander DR.